Biogeosciences, 14, 2929–2953, 2017
https://doi.org/10.5194/bg-14-2929-2017

Biogeosciences
Open Access
EGU

Pore water geochemistry along continental slopes north of the East Siberian Sea: inference of low methane concentrations

Clint M. Miller[1], Gerald R. Dickens[1], Martin Jakobsson[2], Carina Johansson[2], Andrey Koshurnikov[3], Matt O'Regan[2], Francesco Muschitiello[4], Christian Stranne[2], and Carl-Magnus Mörth[2]

[1]Department of Earth Science, Rice University, Houston, TX 77005, USA
[2]Department of Geological Sciences, Stockholm University, 106 91 Stockholm, Sweden
[3]Moscow State University, Geophysics, Moscow, Russian Federation
[4]Lamont–Doherty Earth Observatory, Columbia University, Palisades, NY, USA

Correspondence to: Clint M. Miller (clint.m.miller@rice.edu)

Received: 23 July 2016 – Discussion started: 9 August 2016
Revised: 4 May 2017 – Accepted: 17 May 2017 – Published: 20 June 2017

Abstract. Continental slopes north of the East Siberian Sea potentially hold large amounts of methane (CH_4) in sediments as gas hydrate and free gas. Although release of this CH_4 to the ocean and atmosphere has become a topic of discussion, the region remains sparingly explored. Here we present pore water chemistry results from 32 sediment cores taken during Leg 2 of the 2014 joint Swedish–Russian–US Arctic Ocean Investigation of Climate–Cryosphere–Carbon Interactions (SWERUS-C3) expedition. The cores come from depth transects across the slope and rise extending between the Mendeleev and the Lomonosov ridges, north of Wrangel Island and the New Siberian Islands, respectively. Upward CH_4 flux towards the seafloor, as inferred from profiles of dissolved sulfate (SO_4^{2-}), alkalinity, and the $\delta^{13}C$ of dissolved inorganic carbon (DIC), is negligible at all stations east of 143° E longitude. In the upper 8 m of these cores, downward SO_4^{2-} flux never exceeds 6.2 mol m^{-2} kyr^{-1}, the upward alkalinity flux never exceeds 6.8 mol m^{-2} kyr^{-1}, and $\delta^{13}C$ composition of DIC ($\delta^{13}C$-DIC) only moderately decreases with depth (−3.6 ‰ m^{-1} on average). Moreover, upon addition of Zn acetate to pore water samples, ZnS did not precipitate, indicating a lack of dissolved H_2S. Phosphate, ammonium, and metal profiles reveal that metal oxide reduction by organic carbon dominates the geochemical environment and supports very low organic carbon turnover rates. A single core on the Lomonosov Ridge differs, as diffusive fluxes for SO_4^{2-} and alkalinity were 13.9 and 11.3 mol m^{-2} kyr^{-1}, respectively, the $\delta^{13}C$-DIC gradient was 5.6 ‰ m^{-1}, and Mn^{2+} reduction terminated within 1.3 m of the seafloor. These are among the first pore water results generated from this vast climatically sensitive region, and they imply that abundant CH_4, including gas hydrates, do not characterize the East Siberian Sea slope or rise along the investigated depth transects. This contradicts previous modeling and discussions, which due to the lack of data are almost entirely based on assumption.

1 Introduction

The Arctic is especially sensitive to climate change and has experienced anomalous warming over the last century (Serreze et al., 2000; Peterson et al., 2002; Semiletov et al., 2004; Polyakov et al., 2012). Past and future increases in atmospheric and surface water temperatures should, with time, lead to significant warming of intermediate to deep waters (Dmitrenko et al., 2008; Spielhagen et al., 2011) as well as sediment beneath the seafloor (Reagan and Moridis, 2009; Phrampus et al., 2014). Pore space within the upper few hundred meters of sediment along many continental slopes contains temperature-sensitive methane (CH_4) in the form of gas hydrates, free gas, and dissolved gas (Kvenvolden, 1993, 2001; Beaudoin et al., 2014). Consequently, numerous papers have discussed the potential impact of future warming on CH_4 release from slope sequences of the Arctic Ocean (Paull et al., 1991; Reagan and Moridis, 2008; McGuire et al., 2009; Biastoch et al., 2011; Elliott et al., 2011; Ferré

et al., 2012; Giustiniani et al., 2013; Thatcher et al., 2013; Stranne et al., 2016).

The amount and distribution of CH_4 in sediment along continental slopes remains poorly constrained (Beaudoin et al., 2014). This is particularly true for the Arctic Ocean, because sea-ice cover makes accessibility difficult. Nonetheless, numerous papers have inferred enormous quantities of gas hydrate surrounding the Arctic (Kvenvolden and Grantz, 1990; Max and Lowrie, 1993; Buffett and Archer, 2004; Klauda and Sandler, 2005; Max and Johnson, 2012; Wallmann et al., 2012; Piñero et al., 2013; Figs. 1 and 2). In some sectors, compelling evidence exists for abundant CH_4 and gas hydrate. Bottom-simulating reflectors (BSRs) on seismic profiles generally mark the transition between overlying gas hydrate and underlying free gas (Holbrook et al., 1996; Pecher et al., 2001) and thereby imply high quantities of CH_4 in pore space (Dickens et al., 1997; Pecher et al., 2001). Such BSRs have been documented along the Alaska North Slope (Collett et al., 2010), within the Beaufort Sea (Grantz et al., 1976, 1982; Weaver and Stewart, 1982; Hart et al., 2011; Phrampus et al., 2014), around Canadian Arctic islands (Hyndman and Dallimore, 2001; Majorowicz and Osadetz, 2001; Yamamoto and Dallimore, 2008), adjacent to Svalbard (Posewang and Mienert, 1999; Hustoft et al., 2009; Petersen et al., 2010), and within the Barents Sea (Løvø et al., 1990; Laberg and Andreassen, 1996; Laberg et al., 1998; Ostanin et al., 2013). Furthermore, Lorenson and Kvenvolden (1995) observed high CH_4 concentrations in shelf waters of the Beaufort Sea, and Shakhova et al. (2010a, b) have documented CH_4 escape to the water column above the East Siberian shelf. Sediment on slopes north of the East Siberian Sea potentially contains copious CH_4 and gas hydrate (Fig. 1), although little data supports or refutes this hypothesis.

Regional assessments for abundant CH_4 in marine sediment along continental slopes can be acquired through two general approaches. The first includes geophysical applications, primarily seismic reflection profiling and the recognition of BSRs (Kvenvolden, 1993; Carcione and Tinivella, 2000; Haacke et al., 2008), which are a common, but not ubiquitous, feature of hydrate-bearing sediments. The second utilizes chemical analyses of pore waters obtained from sediment cores (Borowski et al., 1999; D'Hondt et al., 2003). In marine sediments with abundant CH_4, a general process occurs near the seafloor. Microbes utilize upward migrating CH_4 and downward diffusing sulfate (SO_4^{2-}) via anaerobic oxidation of methane (AOM; Barnes and Goldberg, 1976; Boetius et al., 2000):

$$CH_4 + SO_4^{2-} \rightarrow HS^- + HCO_3^- + H_2O. \quad (1)$$

The reaction leads to characteristic pore water chemistry profiles, with a clearly recognizable sulfate–methane transition (SMT; Fig. 3). The depth of the SMT inversely relates to the flux of CH_4, which in turns relates to the distribution of CH_4 beneath the seafloor (Borowski et al., 1999; Dickens, 2001; Bhatnagar et al., 2011). Where CH_4 fluxes toward the seafloor are high, the SMT is located at shallow depth. For example, in cores from the continental shelf and slope of the Beaufort Sea, where seismic profiles indicate gas hydrate, Coffin et al. (2008, 2013) have documented SMTs in shallow sediment (< 10 mbsf).

The joint Swedish–Russian–US Arctic Ocean Investigation of Climate–Cryosphere–Carbon Interactions (SWERUS-C3) project is aimed at understanding spatial changes in carbon cycling across the continental margin north of Siberia. A central theme concerns the amount, distribution, and fluxes of CH_4. The overall project included a two-leg expedition in the boreal summer of 2014 using the Swedish icebreaker IB *Oden*. Between 21 August and 5 October, Leg 2 sailed between Barrow, Alaska, and Tromsø, Norway, including surveys of the continental slope of the East Siberian Sea. SWERUS Leg 2 included geophysical mapping and retrieval of numerous sediment cores, of which 446 pore water samples from 8 piston, 7 gravity, and 17 multicores (Fig. 2) were studied to ascertain potential fluxes of CH_4 toward the seafloor.

2 Background

2.1 East Siberian margin geology

Extensive continental shelves and their associated slopes encircle the Arctic Ocean (Fig. 1). Although only 2.6 % of the world's ocean by area (Jakobsson, 2002), the present Arctic Ocean receives ~ 10 % of global freshwater input (Stein, 2008) as well as a massive discharge of terrigenous material ($> 249\,\mathrm{Mt\,yr^{-1}}$; Holmes et al., 2002). Only Fram Strait (Fig. 1), with a modern sill depth of about 2540 m taken from the International Bathymetric Chart of the Arctic Ocean (Jakobsson et al., 2012), allows deep-water flow to and from the Arctic Ocean. It opened during the early to middle Miocene (Jakobsson et al., 2007; Engen et al., 2008; Hustoft et al., 2009). Prior to this, the Arctic Ocean was connected to other oceans only through shallow seaways (e.g., Turgay Strait), such that deep waters may have been anoxic for long intervals of the Cretaceous and Paleogene (Moran et al., 2006; Sluijs et al., 2006; Jakobsson et al., 2007; O'Regan et al., 2011).

The East Siberian Sea stretches between Wrangel Island to the east and the New Siberian Islands to the west (Fig. 2). The continental shelf within this region is the widest in the world, extending 1500 km north of the coast. North of this expansive shelf lies the continental slope, which connects to the Mendeleev Ridge to the east and the Lomonosov Ridge to the west (Jakobsson et al., 2012). As these slopes lie north of the East Siberian Sea proper, we hereafter refer to them as SNESS for convenience.

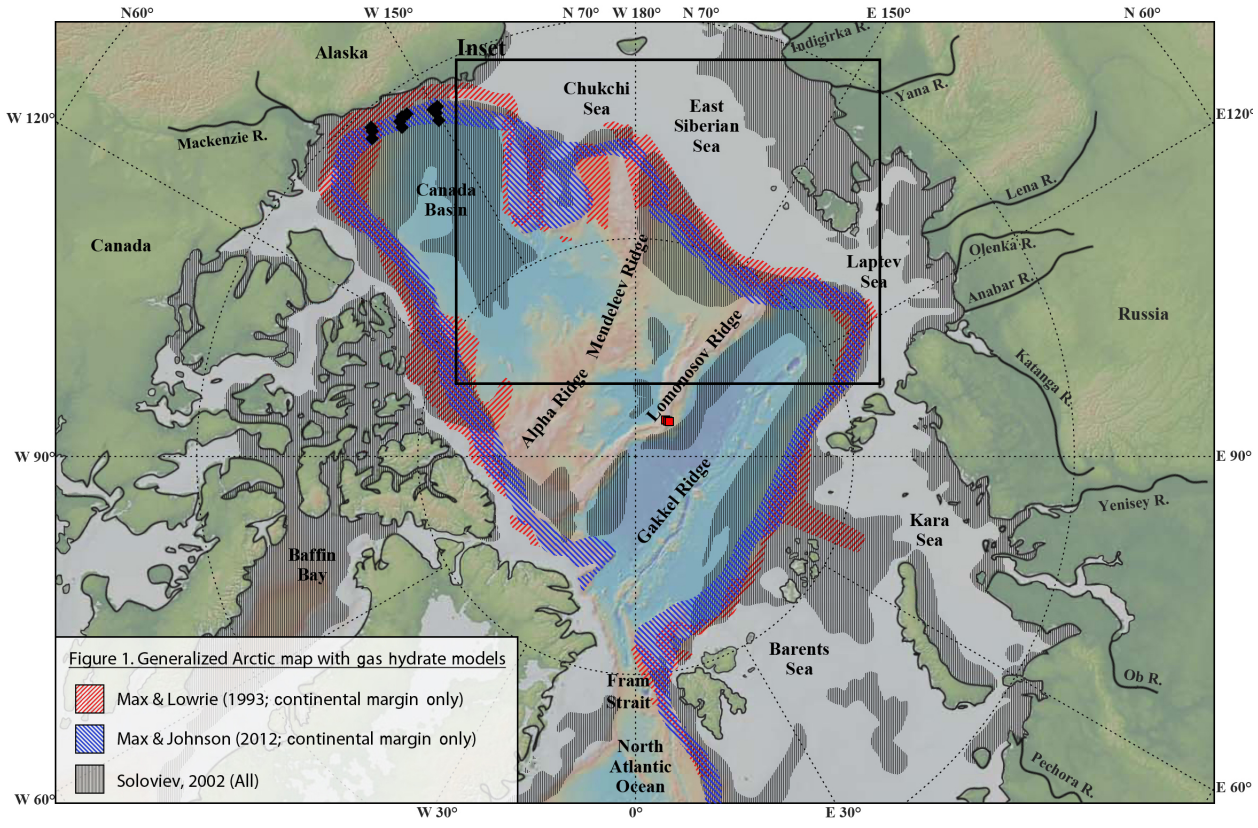

Figure 1. Generalized Arctic map with background from GeoMapApp (http://www.geomapapp.org; Ryan et al., 2009). Observed sulfate–methane transitions during the MITAS 1 expedition shown in black diamonds (Coffin et al., 2013) and Arctic Coring Expedition (ACEX) shown as red squares (Backman and Moran, 2009).

2.2 Regional oceanography

Bottom waters impinging SNESS generally can be divided into three masses: the Pacific halocline (∼ 50–200 m), the Atlantic layer (∼ 200–800 m), and Canada Basin bottom water (> 800 m; Rudels et al., 2000). The Pacific halocline is a cold (−1.5–0° C), low salinity (32–33.5 psu) water mass that serves as a boundary between sea ice and Atlantic layer water (Aagaard, 1981; Aagaard and Carmack, 1989). The underlying Atlantic layer is warmer (> 0 °C) but more saline (33.5–34.5 psu; Rudels et al., 2000). The Atlantic layer originates from water arriving partly through the Fram Strait and partly across the Barents Sea. Canada Basin bottom water is colder (∼ −0.5 °C) and relatively saline (∼ 34.9 psu), with a residence time exceeding 300 years (Stein, 2008). Importantly, inflow from the Atlantic varies over time, which can further influence temperature along slopes of the central Arctic Ocean (Dmitrenko et al., 2009).

2.3 Current speculation on gas hydrates in the Arctic

Even during summer months over the last decade, 2–3 m of sea-ice covers much of SNESS (Stroeve et al., 2012). This necessitates the use of large ice breaking vessels to explore the region. Prior to SWERUS, only four icebreaker expeditions, the 1995 Polarstern expedition ARK-XI/1 (Rachor, 1995), the 1996 Arctic Ocean expedition ARK-XII/1 (Augstein et al., 1997), the 2008 Polarstern expedition ARK-XXIII/3 (Jokat, 2010), and the 2009 Russian–American RUSALCA expedition (Bakhmutov et al., 2009) have retrieved geophysical data and sediment on or adjacent to SNESS. So far, no deep drilling has occurred along SNESS. However, the 2004 Arctic Coring Expedition (ACEX; Backman et al., 2009) drilled and cored the central Lomonosov Ridge (Fig. 1).

Despite the paucity of ground-truth data, many researchers have predicted widespread and abundant CH_4 within SNESS, as clearly shown by maps of inferred Arctic gas hydrate distribution (Fig. 1). This inference has arisen for two main reasons. First, the integrated input of particulate organic carbon (POC) over time provides the ultimate source of CH_4 in marine sediments (Kvenvolden and Grantz, 1990). Arctic slopes may contain high POC contents, which accumulated (a) in shallow platform environments prior to the opening of the Amerasian Basin, (Spencer et al., 2011) (b) during periods of high surface water productivity and oxygen poor bottom water conditions that persisted across much of the Arctic un-

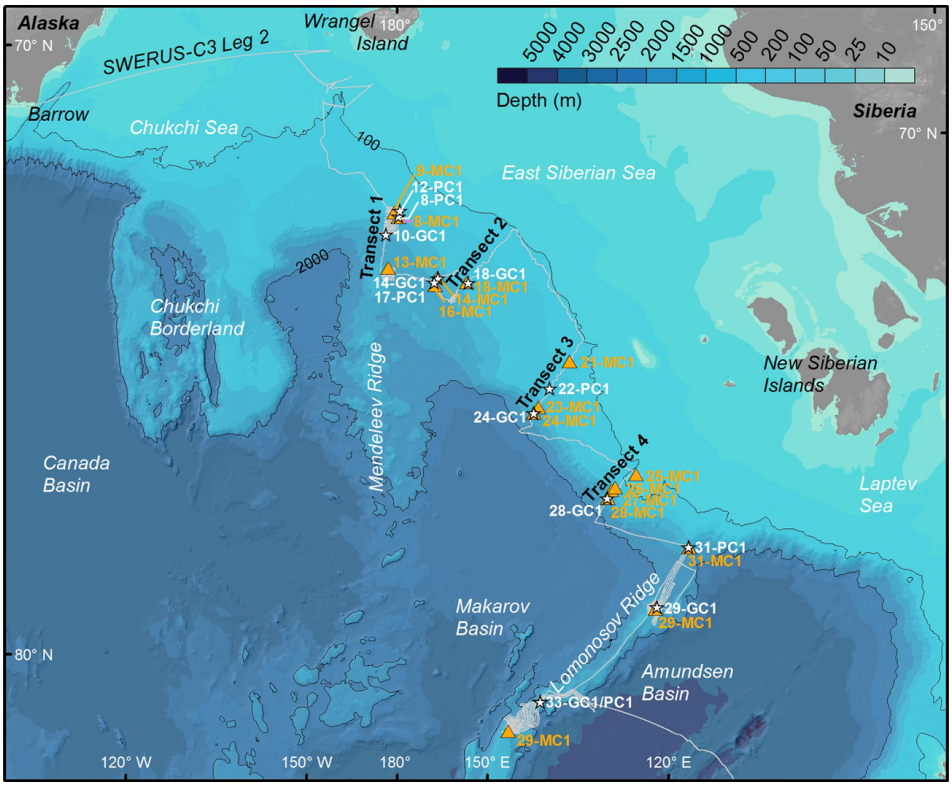

Figure 2. Bathymetric map of Eurasian Arctic showing the overall cruise track of Leg 2 along with the four transects and coring locations. Multicores shown as yellow triangles, gravity and piston cores as white stars, and the ship track line as the gray line from Barrow, Alaska.

til the opening of the Fram Strait in the Neogene (Jakobsson et al., 2007; Stein et al., 2006; O'Regan et al., 2011; Jokat and Ickrath, 2015), or (c) as terrigenous material carried to or deposited along the slopes during interglacial intervals of the Quaternary (Danyushevskaya et al., 1980; Darby et al., 1989; Archer, 2015). Certainly, organic-rich Cretaceous and Eocene sediments have been documented on other Arctic margins and in the ACEX cores on the Lomonosov Ridge (Moran et al., 2006; Backman and Moran, 2009; O'Regan et al., 2011). The second reason is that the thickness of the gas hydrate stability zone depends on bottom water temperature and the geothermal gradient (Dickens, 2001). Because of very low bottom water temperatures along the slope, and generally low regional geothermal gradients (O'Regan et al., 2016), an extensive volume of sediment can host gas hydrate (Miles, 1995; Makogon, 2010).

2.4 Pore water chemistry above methane-charged sediment

Pore water chemistry provides powerful means to constrain CH_4 abundance and fluxes in marine sediment (Borowski et al., 1996; Berg et al., 1998; Jørgensen et al., 2001; Torres and Kastner, 2009; Treude et al., 2014). At locations without significant fluid advection, pore water profiles relate to Fick's law of diffusion and chemical reactions (e.g., Berner, 1977; Froelich et al., 1979; Klump and Martens, 1981; Boudreau, 1997; and Iverson and Jorgensen, 1993). The flux (J) of a dissolved species through porous marine sediment can be calculated from the concentration gradient by (Li and Gregory, 1974; Berner, 1975; Lerman, 1977)

$$J = -\varphi D_s \frac{\partial C}{\partial Z}, \quad (2)$$

where φ is porosity, D_s is the diffusivity of an ion in sediment at a specified temperature, C is concentration, and Z is depth. Note that, as generally written, J is positive for upward fluxes and negative for downward fluxes relative to the seafloor.

At many locations, φ and D_s change only moderately ($< 20\,\%$) in the upper tens of meters below the seafloor. However, abundant CH_4 in sediment leads to a large concentration gradient toward the seafloor and an upward flux of CH_4. The consequent reaction with SO_4^{2-} via AOM (Eq. 1) leads to a series of flux changes in dissolved components (addition or removal) and predictable variations in concentration profiles across an SMT (Alperin et al., 1988; Borowski et al., 1996; Niewohner et al., 1998; Ussler and Paull, 2008; Dickens and Snyder, 2009; Chatterjee et al., 2011). Furthermore, the depth of the SMT directly relates to the flux of CH_4 from below (Jørgensen et al., 1990; Dickens, 2001; D'Hondt et al., 2002;

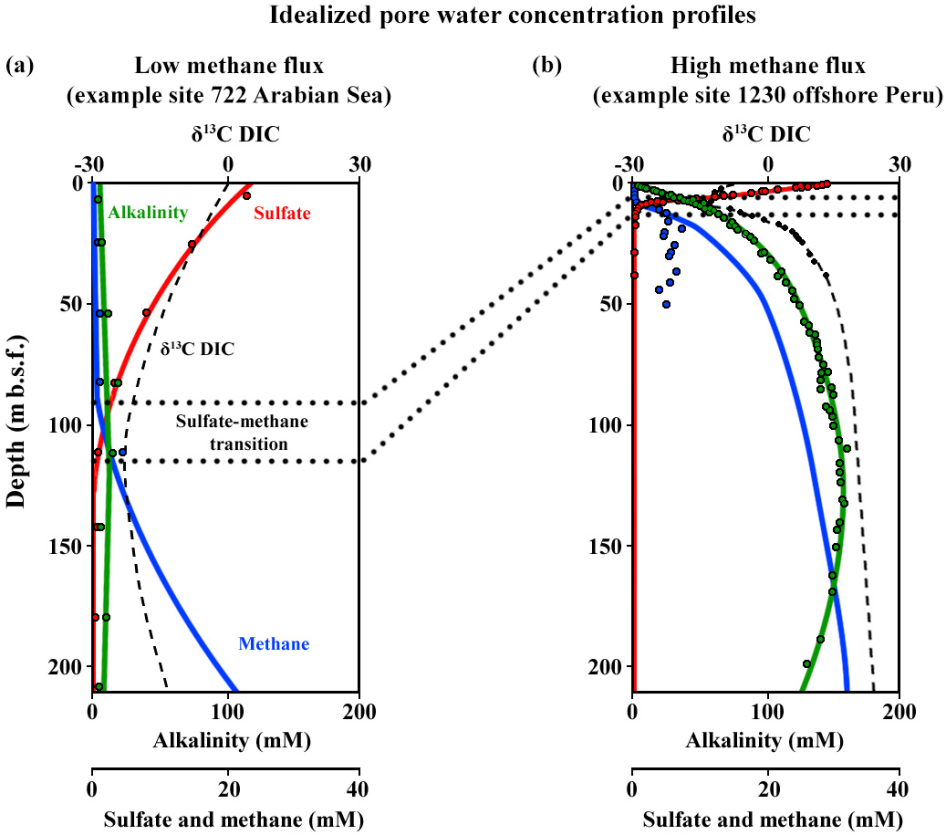

Figure 3. Idealized pore water concentration profiles for high and low upward methane flux. Discrete data points for sites 722 (Arabian Sea; Seifert and Michaelis, 1991; D'Hondt et al., 2002) and 1230 (offshore Peru; Donohue et al., 2006) are given as reference.

Hensen et al., 2003), largely because SO_4^{2-} concentrations at the seafloor are nearly constant throughout the oceans.

Large areas of continental slopes across the world host CH_4 in sediment and consequently have a prominent SMT (D'Hondt et al., 2002). This feature is generally within the upper 30 m beneath the seafloor and is characterized as a thin (< 3 m) horizon with major inflections in both CH_4 and SO_4^{2-} profiles (Fig. 3). Sulfate concentrations decrease from seawater values at the seafloor to near zero at the SMT; by contrast, CH_4 concentrations rise from zero at the SMT to elevated values at depth.

Importantly, though, as one can infer from Eqs. (1) and (2), AOM affects additional species dissolved in pore water (Alperin et al., 1988; Jørgensen et al., 1990; Dickens, 2001; Hensen et al., 2003; Snyder et al., 2007). Dissolved HS^- and HCO_3^- concentrations necessarily increase across the SMT, so an inflection occurs in their concentration profiles. These two species contribute to total alkalinity of marine waters (Gieskes and Rogers, 1973; Haraldsson et al., 1997), which can be defined as

$$\mathrm{Alk}_T = \left[\mathrm{HCO_3^-}\right] + 2\left[\mathrm{CO_3^{2-}}\right] + \left[\mathrm{HS^-}\right] + \left[\mathrm{B(OH)_4^-}\right] + \left[\mathrm{OH^-}\right] + \left[\mathrm{HPO_4^{2-}}\right] + [\mathrm{NH_3}] + [X]\,, \quad (3)$$

where X refers to several minor species. However, in shallow sediments found above almost all CH_4-charged systems, this can be expressed as

$$\mathrm{Alk}_T \approx \left[\mathrm{HCO_3^-}\right] + \left[\mathrm{HS^-}\right]. \quad (4)$$

Therefore, because of the production of HS^- and HCO_3^-, an inflection in Alk_T occurs across the SMT (Luff and Wallmann, 2003; Dickens and Snyder, 2009; Jørgensen and Parkes, 2010; Chatterjee et al., 2011; Smith and Coffin, 2014; Ye et al., 2016).

Marked changes in pore water profiles of other components also typically occur across the SMT (Fig. 3). Because CH_4 is greatly depleted in ^{13}C, due to isotope fractionation during methanogenesis at depth (Whiticar, 1999; Paull et al., 2000), the conversion of CH_4 to HCO_3^- (Eq. 1) decreases the $\delta^{13}C$ of DIC across the SMT (Torres et al., 2007; Holler et al., 2009; Chatterjee et al., 2011; Yoshinaga et al., 2014). However, the magnitude of this change in $\delta^{13}C$ composition of

DIC (δ^{13}C-DIC) is complicated because excess ^{13}C-enriched HCO_3^- (formed during methanogenesis and subsequent reactions) can also rise from below (Snyder et al., 2007; Chatterjee et al., 2011). Dissolved Ba^{2+} concentrations generally increase significantly just above the SMT. This is because solid barite ($BaSO_4$), a ubiquitous component of marine sediment on continental slopes (Dymond et al., 1992; Gingele and Dahmke, 1994), dissolves in the SO_4^{2-}-depleted pore water, and dissolved Ba^{2+} then diffuses back across the SMT (Dickens, 2001; Riedinger et al., 2006; Nöthen and Kasten, 2011). Dissolved Ca^{2+} concentrations usually decrease across the SMT. This is due to authigenic carbonate precipitation resulting from the production of excess HCO_3^- (Greinert et al., 2001; Luff and Wallmann 2003; Snyder et al., 2007). Conversely, dissolved NH_4^+ concentrations exhibit no inflection across the SMT. This is because while decomposition of particulate organic matter (POM) generates NH_4^+, AOM does not (Borowski et al., 1996).

Studies at numerous locations demonstrate that characteristic pore water profiles delineate sediment sequences with significant CH_4, including gas hydrate, in the upper few hundred meters below the seafloor (Fig. 3). Good examples include the Baltic Sea (Jørgensen et al., 1990), Black Sea (Jørgensen et al., 2004), Blake Ridge (Paull et al., 2000; Borowski et al., 2001), Cariaco Trench (Reeburgh, 1976), Cascadia margin (Torres and Kastner, 2009), Gulf of Mexico (Kastner et al., 2008a; Hu et al., 2010; Smith and Coffin, 2014), Hydrate Ridge (Claypool et al., 2006), offshore Namibia (Niewohner et al., 1998), offshore Peru (Donohue et al., 2006), South China Sea (Luo et al., 2013; Hu et al., 2015), and Sea of Japan (Expedition Scientists, 2014). Moreover, in regions dominated by diffusion, fluxes of dissolved CH_4 can be estimated using Eq. (2) from concentration profiles of multiple constituents (e.g., SO_4^{2-}, HCO_3^-, Ca^{2+}) and knowledge of porosity and sedimentary diffusion constants (e.g., Niewohner et al., 1998; Snyder et al., 2007). At sites with abundant CH_4 in the upper few hundred meters below the seafloor, notably including sites with gas hydrate and sites in the Beaufort Sea, estimated values for J^{CH_4} and $-J^{SO_4^{2-}}$ are universally high ($> \sim 50\,\mathrm{mol\,m^{-2}\,kyr^{-1}}$).

It should be noted that at seafloor locations with significant upward advection of fluids, such as at seeps and vents, the aforementioned reactions occur, but the pore water profiles become more complicated to model (Berner, 1980; Torres et al., 2002; Chatterjee et al., 2011). This is because the advecting fluids typically have different chemistry than surrounding sediment (even if charged with CH_4) and because advection often involves multiphase fluid flow (free gas and liquid) that may be episodic. Nonetheless, at least on continental slopes, if the upward advecting fluids contain significant CH_4 (even as gas bubbles), a prominent SMT occurs but is shoaled toward the seafloor with respect to predictions based on CH_4 diffusion alone (Luff and Wallmann, 2003; Kastner et al., 2008a). Indeed, at locations where CH_4 gas bubbles escape the seafloor, the SMT lies at the seafloor (e.g., Aharon and Fu, 2000; Joye et al., 2004; Hu et al., 2010).

3 Materials and methods

3.1 SWERUS-C3 expedition, Leg 2

Leg 2 of SWERUS-C3 included four transects across the SNESS (Fig. 2). These transects were along Arlis Spur (Tr1), the north of central east Siberia (Tr2), from close to Henrietta Island to the Makarov Basin (Tr3), and on the Amerasian side of the Lomonosov Ridge (Tr4). Along each transect, scientific operations involved bathymetric mapping as well as sediment coring at stations. An additional coring station was located on the Lomonosov Ridge, near its intersection with the Siberian margin.

An array of coring techniques were used along each transect. In total, 50 sediment cores were collected at 34 stations. These included multicore sets (22), gravity cores (23), piston cores (11), and kasten cores (2). The multicorer was an eight-tube corer built by Oktopus GmbH. The polycarbonate liners were 60 cm long with a 10 cm diameter. The piston and gravity coring system was built by Stockholm University with an inner diameter of 10 cm. Trigger weight cores were also collected during piston coring. The different coring systems enabled sediment and pore water collection from the seafloor to upwards of 9 m below the seafloor (mbsf).

3.2 Core material

For gravity and piston cores, physical properties were analyzed on the ship using a Geotek Multi-Sensor Core Logger (MSCL). These included measurements of the gamma-ray derived bulk density, compressional wave velocity (P wave), and magnetic susceptibility at 1 cm resolution. Discrete samples (2–3 per section) were taken for sediment index property measurements (bulk density, porosity, water content, and grain density). Grain density was measured using a helium displacement pycnometer on oven-dried samples. Porosity profiles were generated using the smoothed (3 pt) MSCL-derived bulk density (ρ_b) and the average grain density (ρ_g) from each core, where

$$\varphi = \frac{(\rho_g - \rho_b)}{(\rho_b - \rho_f)}, \quad (5)$$

and the pore fluid density (ρ_f) was assumed to be $1.024\,\mathrm{g\,cm^{-3}}$.

3.3 Interstitial water collection

Cores were cut into ~ 1.5 m long sections immediately on the ship deck, brought to the geochemistry laboratory, and placed on precut racks. Laboratory temperature was a near constant 22 °C. Pore waters were collected using Rhizon samplers

Table 1. Quality assurance and quality control (QA/QC).

Analysis	Sample type	Number	Result
Alkalinity	Spiked	15	PE = 1.53 %
Alkalinity	Duplicate	8	PD = 1.30 %
δ^{13}C-DIC	Seawater standard	2	0.23 and 0.32 ‰
δ^{13}C-DIC	Blind field duplicate	4	PD = 22.98 %
δ^{13}C-DIC	Field blank	1	No result
δ^{13}C-DIC	Duplicate	10	PD = 14.70 %
Metals	Spiked	51	RSD = 2.55 % (Ba), 2.17 % (Ca), 1.53 % (Fe), 0.77 % (Mg), 1.73 % (Mn), 1.88 % (S), and 1.42 % (Sr)
Metals	Blind field duplicate	11	PD = 2.56 % (Ba), 3.77 % (Ca), 5.81 % (Fe), 2.68 % (Mg), 3.07 % (Mn), 0.71 % (S), and 3.79 % (Sr)
Metals	Field blank	2	BDL
Phosphate	VKI standard	2	PE = 1.28 and 2.69 %
Ammonia	VKI standard	2	PE = 2.40 and 6.25 %

Notes: PE = percent error; PD = percent difference; RSD = relative standard deviation; BDL = below detection limit.

(Seeberg-Elverfeldt et al., 2005; Dickens et al., 2007). Sampling involved drilling holes through the core liner, inserting Rhizons into the sediment core, and obtaining small volumes of pore water via vacuum and "microfiltration." The Rhizons used were 5 cm porous flat tip male Luer locks (19.21.23) with 12 cm tubing, purchased from Rhizosphere Research Products (www.rhizosphere.com).

In total, 529 pore water samples were collected from 32 cores, which ranged from 0.16 to 8.43 m in length (Table S2 in the Supplement). Rhizons in gravity and piston cores typically were spaced every 20 to 30 cm. Because the use of Rhizon sampling for collecting pore waters of deep-sea sediments remains a relatively novel and engaging topic (Dickens, 2007; Xu et al., 2012; Miller et al., 2014), we discuss the procedure in detail, as well as several experiments regarding our sampling, in the Supplement.

While in the shipboard laboratory, Rhizon samples were divided into six aliquots when sufficient water was available. This sample splitting led to 2465 aliquots of pore water in total, which then could be examined for different species at different laboratories. Aliquots 1, 3, and 6 (below) were collected for all 32 cores.

3.4 Interstitial water analyses

The first aliquot was used to measure Alk_T using a Mettler Toledo titrator on IB *Oden*. Immediately after collection, pore water was diluted with Milli-Q water and auto-titrated. Fifteen spiked samples and eight duplicates were analyzed onboard for quality control. Spiked samples were created by pipetting certified reference material (Batch 135; www.cdiac.ornl.gov/oceans/Dickson_CRM) into Milli-Q water. Results for spiked samples and duplicates are reported in Table 1.

The second aliquot was used to measure the δ^{13}C composition of DIC. Septum-sealed glass vials prepared with H_3PO_4 and flushed with helium were prepared before the expedition. Samples were sealed in boxes and refrigerated for the remainder of the cruise. Four field duplicates, two seawater standards, and a field blank were collected, stored, and analyzed with the samples. The δ^{13}C-DIC analyses were performed on a Gasbench II coupled to a MAT 253 mass spectrometer (both Thermo Scientific) at Stockholm University. The δ^{13}C-DIC is reported in conventional delta notation relative to Vienna PeeDee Belemnite (VPDB). Results for field duplicates and standards are reported in Table 1. Standard deviation for the analyses of δ^{13}C-DIC was less than 0.1 ‰.

The third aliquot was used to measure dissolved sulfur and metal concentrations. Samples were acid preserved with 10 µL ultrapure HNO_3. Additionally, 11 blind field duplicates and 2 field blanks were collected and processed in the same manner. Concentrations of Ba, Ca, Fe, Mg, Mn, S, and Sr were determined on an Agilent Vista Pro inductively coupled plasma atomic emission spectrometer (ICP-AES) in the geochemistry facilities at Rice University. Known standard solutions and pore fluid samples were diluted 1 : 20 with 18 MΩ water. Scandium was added to both standards and samples to correct for instrumental drift (emission line 361.383 nm). Wavelengths used for elemental analysis followed those indicated by Murray et al. (2000). Following initial analysis, an additional dilution, 1 : 80 with 18 MΩ water, was analyzed for Ca, Mg, and S. After every 10 analyses, an International Association for the Physical Sciences of the Oceans (IAPSO) standard seawater spiked sample and a blank were examined for quality control. Relative standard deviations (RSD) from stock solutions are reported in Table 1.

The fourth aliquot was used to measure dissolved ammonia (NH_4^+) via a colorimetric method similar to that presented by Gieskes et al. (1991). Set volumes of pore water were pipetted into cuvettes and diluted with Milli-Q water. Two reagents were then pipetted into the cuvettes.

Reagent A was prepared by adding $Na_3C_6H_5O_7$, C_6H_5OH, and $Na_2(Fe(CN)_5NO)$ to Milli-Q water. Reagent B was prepared by dissolving NaOH in Milli-Q water and adding NaClO solution. Solutions were mixed and allowed to react for at least 6 but not more than 24 h. Solutions turned various shades of blue, which to relate to NH_4^+ concentration, and were measured by absorbance at 630 nm on a Hitachi U-1100 spectrophotometer. Five-point calibration curves were measured before each sample set and corrected using the VKI standard (QC RW1; www.eurofins.dk; Table 1).

The fifth aliquot was used to measure dissolved phosphate (PO_4^{3-}) following the method given by Gieskes et al. (1991). Remaining pore water (generally between 1 and 3 mL) was added to Milli-Q water to a sum of 10 mL. Two reagents were added to the solution to react with PO_4^{3-}. Reagent A was prepared by making three solutions: $(NH_4)_2MoO_4$, H_2SO_4, and $C_8H_4K_2O_{12}Sb_2 \cdot XH_2O$ were added to Milli-Q water, and the solutions were added dropwise. Reagent B was created with $C_6H_8O_6$. After samples were prepared, reagents A and B were added, mixed, and allowed to react for 30 min. Solutions turned various shades of blue, relating to PO_4^{3-} concentration, and were measured at an absorbance of 880 nm. Five-point calibration curves were measured before each sample set and corrected using the VKI standard.

For 352 pore water samples, a sixth aliquot of approximately 2 mL was mixed with 200 µL of a 2.5 % Zn-acetate ($Zn(C_2H_3O_2)_2$) solution. Given the extremely low solubility of ZnS, a white precipitate forms when such a solution is added to pore water samples with even trace H_2S concentrations (Cline, 1969; Goldhaber, 1974).

For the ICP-AES analyses, a method detection limit (MDL) can be determined as follows:

$$\mathrm{MDL} = \frac{(C_{\mathrm{High}} - C_{\mathrm{Low}})}{(I_{\mathrm{High}} - I_{\mathrm{Low}})} 3\sigma\,, \tag{6}$$

where C = concentration and I = intensity (counts per second on the ICP-AES). The MDLs were as follows: Ba = 0.01 µM, Ca = 0.08 µM, Fe = 5.9 µM, Mg = 0.22 µM, Mn = 0.24 µM, S = 1.2 µM, and Sr = 0.01 µM. On all plots, for reference, we place dashed lines for values of the IAPSO seawater standard (Alkalinity = 2.33 mM, Ba = 0.00 mM, Ca = 10.28 mM, Fe = 0.00 mM, Mg = 53.06 mM, Mn = 0.00 mM, S = 28.19 mM, Sr = 0.09 mM, NH_4^+ = 0.00 mM, and HPO_4^{2-} = 0.00 mM).

4 Results

4.1 General observations

With the large number of pore water measurements (Table S1 in the Supplement), we begin with some generalities regarding results. We plot pore water concentration profiles along each transect collectively (Figs. 4–8), irrespective of coring device or water depth, although clear variance in pore water chemistry exists between stations for some dissolved species (e.g., Fe).

Most species display "smooth" concentration profiles with respect to sediment depth (Figs. 4–8). That is, concentrations of successive samples do not display a high degree of scatter. This is expected for pore water profiles in sediment where diffusion dominates (Froelich et al., 1979; Klump and Martens, 1981; Schulz, 2000; Torres and Kastner, 2009; Hu et al., 2015). However, for some dissolved species whose concentrations do not appreciably change over depth (e.g., Ba^{2+} and Ca^{2+}), scatter exists beyond that predicted from analytical precision. We discuss this in the Supplement.

4.2 Alkalinity and δ^{13}C of DIC

Alkalinity concentrations increase with depth in all cores (Figs. 4–8). Moreover, in most cases, the rise is roughly linear. Across all stations on the four transects, alkalinity increases by an average of 0.51 mM m^{-1}, although variance exists between mean gradients for each transect (Tr1 = 0.46 mM m^{-1}, Tr2 = 0.34 mM m^{-1}, Tr3 = 0.91 mM m^{-1}, and Tr4 = 0.44 mM m^{-1}) and by station along each transect. The Lomonosov Ridge station differs (Fig. 8), as alkalinity increases much more with depth (1.86 mM m^{-1}).

Concave-down δ^{13}C-DIC profiles characterize pore waters at all stations (Figs. 4–8). The decrease in δ^{13}C-DIC is most pronounced near the seafloor. Across all stations along the four transects, pore water δ^{13}C-DIC values decrease from near zero close to the mud line at an average of −3.6 ‰ m^{-1}. Again, variance in mean gradients occurs between stations and transects (Tr1 = −3.3 ‰ m^{-1}, Tr2 = −3.0 ‰ m^{-1}, and Tr3 = −4.7 ‰ m^{-1}). As with alkalinity, the δ^{13}C-DIC profile at the Lomonosov Ridge station differs, with values decreasing by 5.6 ‰ m^{-1}, such that by 8 mbsf δ^{13}C-DIC approaches −45 ‰. In summary, a basic relationship exists between higher alkalinity and lower δ^{13}C-DIC across all stations.

4.3 Sulfur and sulfate

No sulfide was observed by smell, and no ZnS precipitated in any pore water sample upon addition of Zn-acetate solution. Molar concentrations of total dissolved sulfur should, therefore, represent those of dissolved SO_4^{2-}. Along the four transects, dissolved sulfur concentrations decrease with depth at all stations (Figs. 4–7). The total dissolved sulfur concentrations in the shallowest samples varied from 27.3 to 30.6 mM and averaged 28.7 mM. From these "seafloor" values, concentrations decrease by an average 0.69 mM m^{-1}, again with variance according to stations and transect (Tr1 = −0.58 mM m^{-1}, Tr2 = −0.57 mM m^{-1}, Tr3 = −1.09 mM m^{-1}, and Tr4 = −0.60 mM m^{-1}). The dissolved sulfur gradients across all stations within SNESS range from −0.41 to −1.13 mM m^{-1}. Dissolved sulfur at the Lomonosov Ridge station displays a significantly steeper

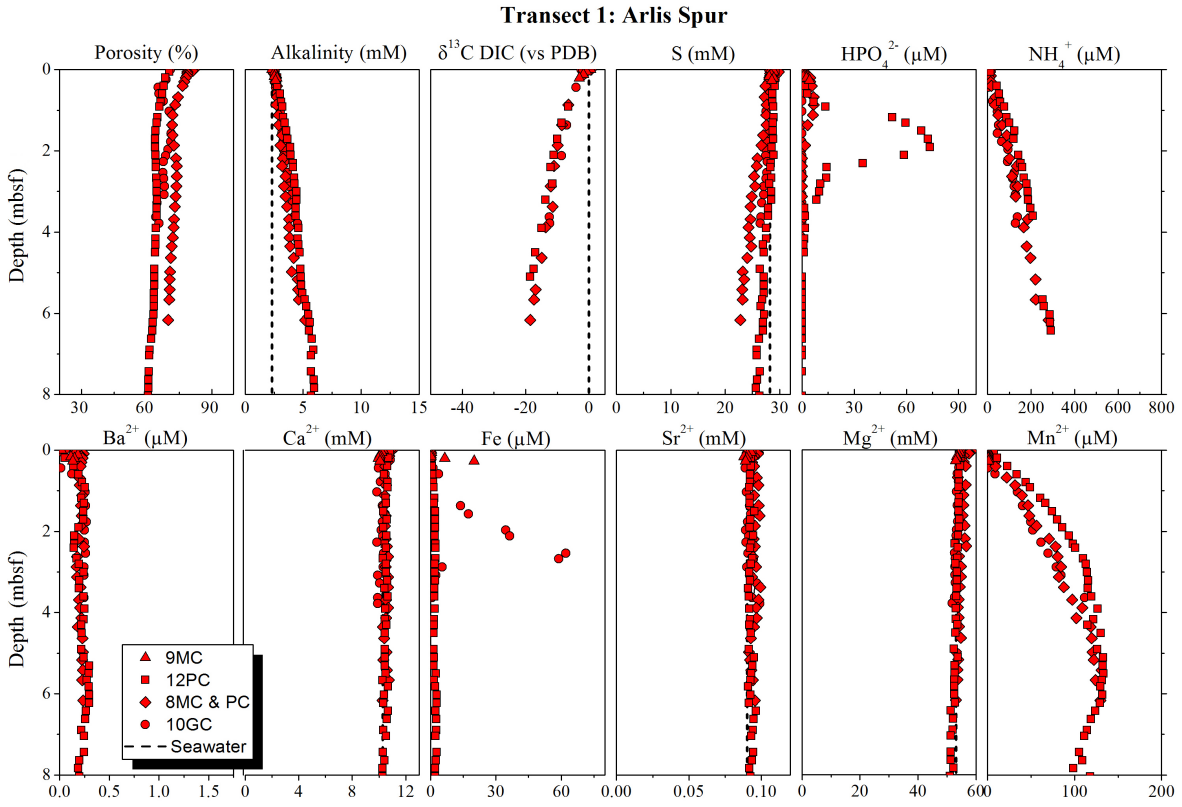

Figure 4. Transect 1 results. IAPSO standard seawater (black dotted line) shown for comparison.

decrease than any other station ($-1.92\,\mathrm{mM\,m^{-1}}$). Importantly, decreases in dissolved sulfur are similar in magnitude to increases in alkalinity at each station examined. Indeed, the molar ratio of alkalinity change to sulfur change ($-\Delta\mathrm{Alkalinity}/\Delta\mathrm{S}$) is 0.98 (Fig. 9a).

4.4 Ammonia and phosphate

The C : N : P molar ratio of typical marine organic matter is approximately 106 : 16 : 1 (Redfield, 1958; Takahashi, 1985). Although this ratio differs for terrestrial organic carbon (closer to 134 : 9 : 1, Tian et al., 2010), dissolved NH_4^+ and HPO_4^{2-} concentrations in pore water can be used in a general sense to assess consumption of particulate organic carbon. This is because the degradation releases these species to pore water (Froelich et al., 1979). Notably, concentrations of NH_4^+ and HPO_4^{2-} are near or below detection in samples immediately below the seafloor (Figs. 4–8).

Dissolved NH_4^+ profiles increase almost linearly with depth, although with slight concave-down curvature. Similar to alkalinity profiles, NH_4^+ concentrations rise with depth below the seafloor and more at stations with shallower water depth (although we note an exception for Tr2). Across stations along the four transects, pore water NH_4^+ concentrations increase with depth on average by $38.69\,\mu\mathrm{M\,m^{-1}}$, with a range from 11.3 to $76.1\,\mu\mathrm{M\,m^{-1}}$. Along each transect, the average NH_4^+ gradients are as follows: Tr1 $= 43.0\,\mu\mathrm{M\,m^{-1}}$, Tr2 $= 17.4\,\mu\mathrm{M\,m^{-1}}$, Tr3 $= 69.0\,\mu\mathrm{M\,m^{-1}}$, and Tr4 $= 29.0\,\mu\mathrm{M\,m^{-1}}$.

By contrast, concentrations of dissolved HPO_4^{2-} in our cores typically increase to a subsurface maximum and then decrease (Figs. 4–8). Based on the available data, a more pronounced maximum appears to occur at stations with relatively shallow water depth. For example, consider the peak in HPO_4^{2-} concentrations at four stations. At the two shallow stations, S12 (384 m) and S22 (367 m), the HPO_4^{2-} maxima are 73 μM (1.91 m) and 18 μM (0.66 m), respectively, but at the two deeper stations, S17 (977 m) and S14 (733 m), the HPO_4^{2-} maxima are only 6.7 μM (1.76 m) and 7.1 μM (2.33 m), respectively. The station on the Lomonosov Ridge (S31) has a high in HPO_4^{2-} concentration of 76 μM at 1.02 m below the seafloor. In general, stations with more pronounced HPO_4^{2-} maxima also have greater increases in alkalinity with depth.

The NH_4^+, HPO_4^{2-}, and alkalinity profiles relate to one another statistically, although with some distinctions. All stations have a C : N ratio in pore waters much higher than the canonical Redfield ratio of 6.625 (Fig. 10). Alternatively, the concentration relationship of alkalinity and ammonium ion can be expressed by a second order polynomial ($[NH_4^+] = -0.003[\mathrm{Alk}]2 + 0.105\ [\mathrm{Alk}] - 0.253$; Fig. 9b) with an

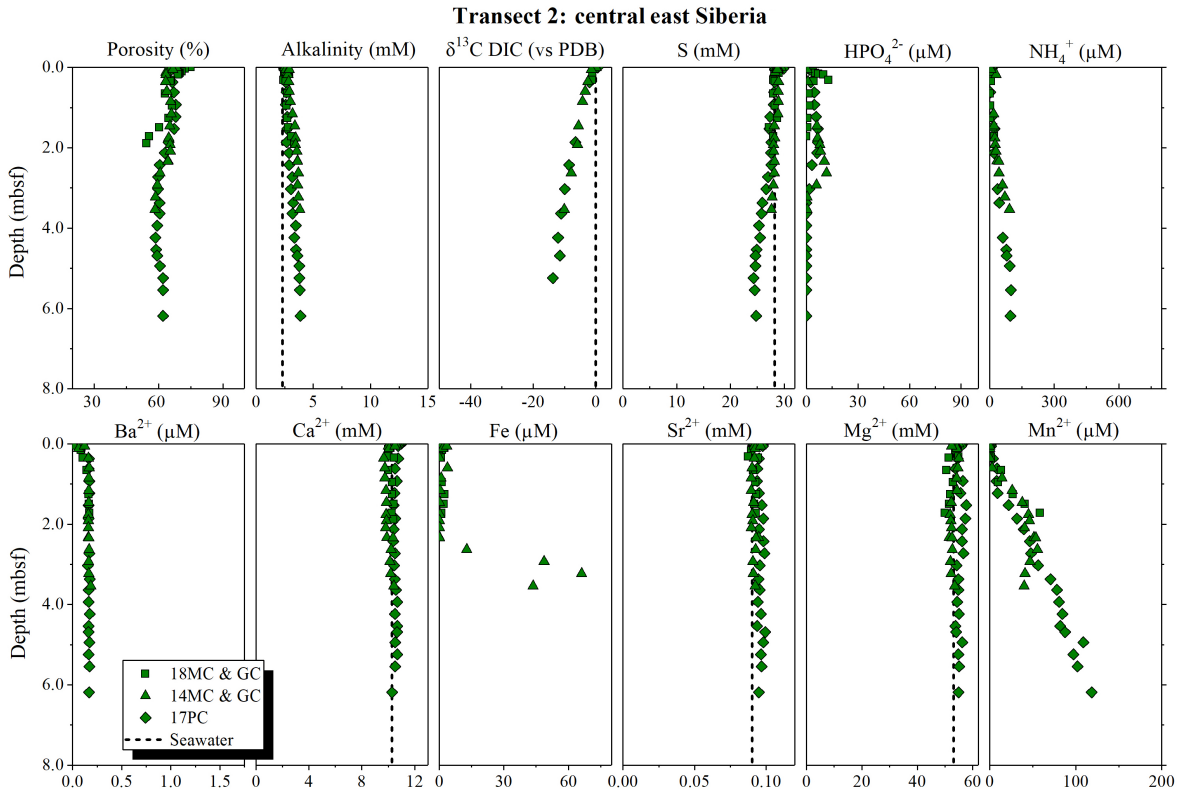

Figure 5. Transect 2 results. IAPSO standard seawater (black dotted line) shown for comparison.

average molar ratio (Alk / NH_4^+) of 14.7, which is close to that expected for degradation of terrestrial organic carbon. Interestingly, this ratio deviates somewhat across transects, increasing at sites from Tr1, Tr3, and Tr2, to the Lomonosov Ridge station. Across all stations and above the subseafloor HPO_4^{2-} peak, the molar ratio of alkalinity to phosphate ion (Alk / HPO_4^{2-}) averages 55.7 in pore water samples. This ratio also generally increases in cores from east to west.

4.5 Metals

At most stations, dissolved Ba^{2+} concentrations increase nonlinearly from values at or below detection limit (0.01 µM) near the seafloor to generally constant values (0.6–0.7 µM) within 0.8 m below the seafloor. However, at several stations, dissolved Ba^{2+} concentrations remain at or below the detection limit for all samples.

Overall, dissolved Ca^{2+}, Mg^{2+}, and Sr^{2+} concentrations decrease with depth (Figs. 4–8). For the stations along the four transects, Ca^{2+} concentrations drop on average between -0.09 and $-0.12\,mM\,m^{-1}$ (Tr1), about $-0.09\,mM\,m^{-1}$ (Tr2), between −0.09 and −0.10 (Tr3), and $-0.075\,mM\,m^{-1}$ (Tr4). Magnesium concentrations also drop, with the average change being between −0.43 and $-0.48\,mM\,m^{-1}$ (Tr1), between −0.27 and −1.32 (Tr2), between −0.86 and $-0.94\,mM\,m^{-1}$ (Tr3), and $-0.467\,mM\,m^{-1}$ (Tr4). Strontium concentrations decrease by an average of $0.3\,\mu M\,m^{-1}$, considering all stations along the four transects (Tr1 = $0.5\,\mu M\,m^{-1}$, Tr2 = $0.3\,\mu M\,m^{-1}$, Tr3 = $0.1\,\mu M\,m^{-1}$, and Tr4 = $0.1\,\mu M\,m^{-1}$). The station on the Lomonosov Ridge again stands apart. At this location, the decreases in dissolved Ca^{2+}, Mg^{2+}, and Sr^{2+} are $0.27\,mM\,m^{-1}$, $1.24\,mM\,m^{-1}$, and $0.50\,\mu M\,m^{-1}$, respectively.

The profiles of dissolved Mn and Fe are complicated in terms of location. Generally, profiles show a broad rise in concentrations within the upper sediment and a subsequent drop in concentrations at deeper depth. Some stations have a maxima in dissolved Mn (Stations S12 (135 µM at 5 m), S28 (66 µM at 3.1 m), and the Lomonosov Ridge (86 µM at 1.3 m), where concentrations decrease below. At other stations, however, Mn concentrations still appear to be increasing at the lowest depth. Iron concentrations are generally below the detection limit at or near the seafloor, and begin increasing around 2.5–3.5 m, reaching concentrations upward of 20 µM.

5 Discussion

5.1 Fidelity of Rhizon pore water measurements

Researchers have employed multiple methods to extract pore waters from marine sediments over the last few decades, but

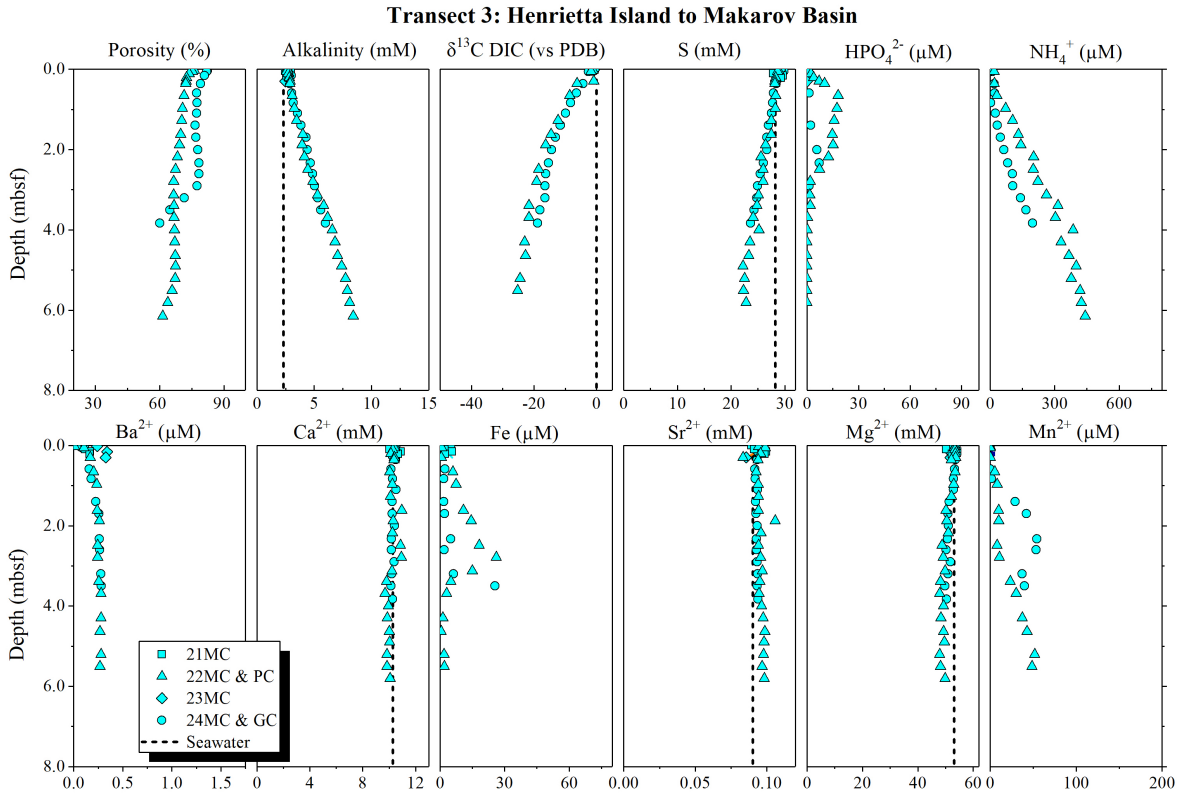

Figure 6. Transect 3 results. IAPSO standard seawater (black dotted line) shown for comparison.

the Rhizon technique remains relatively novel (e.g., Seeberg-Elverfeldt et al., 2005; Dickens et al., 2007; Pohlman et al., 2008). Several studies have questioned the accuracy and precision of analyses obtained through this approach (e.g., Schrum et al., 2012; Miller et al., 2014). Two experiments conducted during the SWERUS-C3 Leg 2 expedition using the Rhizons suggest that part of the problem concerns the timing and location of sampling (Supplement). Notably, however, as clearly documented in previous works (Seeberg-Elverfeldt et al., 2005; Dickens et al., 2007; Pohlman et al., 2008), Rhizon sampling can lead to smooth concentration profiles for multiple dissolved species, including alkalinity (Figs. 4–8).

Concerns about Rhizon sampling may be valid for dissolved components when concentration gradients are very low. For example, Schrum et al. (2012) stressed alkalinity differences between samples collected at similar depth using Rhizon sampling and conventional squeezing. However, the total alkalinity range in this study was between 1.6 and 2.6 mM, and typical differences were 0.06 mM. A similar finding occurs in the dissolved Ca^{2+} and Ba^{2+} profiles of this study, where the range in values is small and adjacent samples deviate by more than analytical precision (Table 1, Fig. S3). However, when the signal-to-noise ratio becomes high, as is true with most dissolved components at most stations (Figs. 4–8), the Rhizon sampling renders pore water profiles with well-defined concentration gradients that can be interpreted in terms of chemical reactions and fluxes.

5.2 General absence of methane

Direct measurements of dissolved CH_4 in deep-sea sediment are complicated (Claypool and Kvenvolden, 1983). During core retrieval and depressurization, major CH_4 loss can occur from pore space (Dickens et al., 1997). Importantly, in sediments recovered through piston coring and where in situ CH_4 concentrations significantly exceed solubility conditions at 1 atm pressure, gas release typically generates sub-horizontal cracks ("gas voids") that span the core between the liner. No such cracks were documented in any of the cores.

Excluding station 31 on the Lomonosov Ridge, there is no indication of a shallow SMT in any of the cores. Interstitial water sulfur concentrations do not drop below 22.8 mM within the upper 8 m. In fact, calculated downward SO_4^{2-} fluxes, as inferred from sulfur concentration gradients (Table 2), range from -1.8 to $-6.2\,mol\,m^{-2}\,kyr^{-1}$ for all stations except Station S31. For comparison, for a site with a near-seafloor temperature of 2 °C (Fig. S2) and porosities similar to those measured (Fig. S1), an SMT at 6.0 mbsf would imply an SO_4^{2-} flux of $-40\,mol\,m^{-2}\,kyr^{-1}$.

Given the lack of HS^- and the measured pH (Fig. S2), alkalinity should closely approximate HCO_3^- concentrations

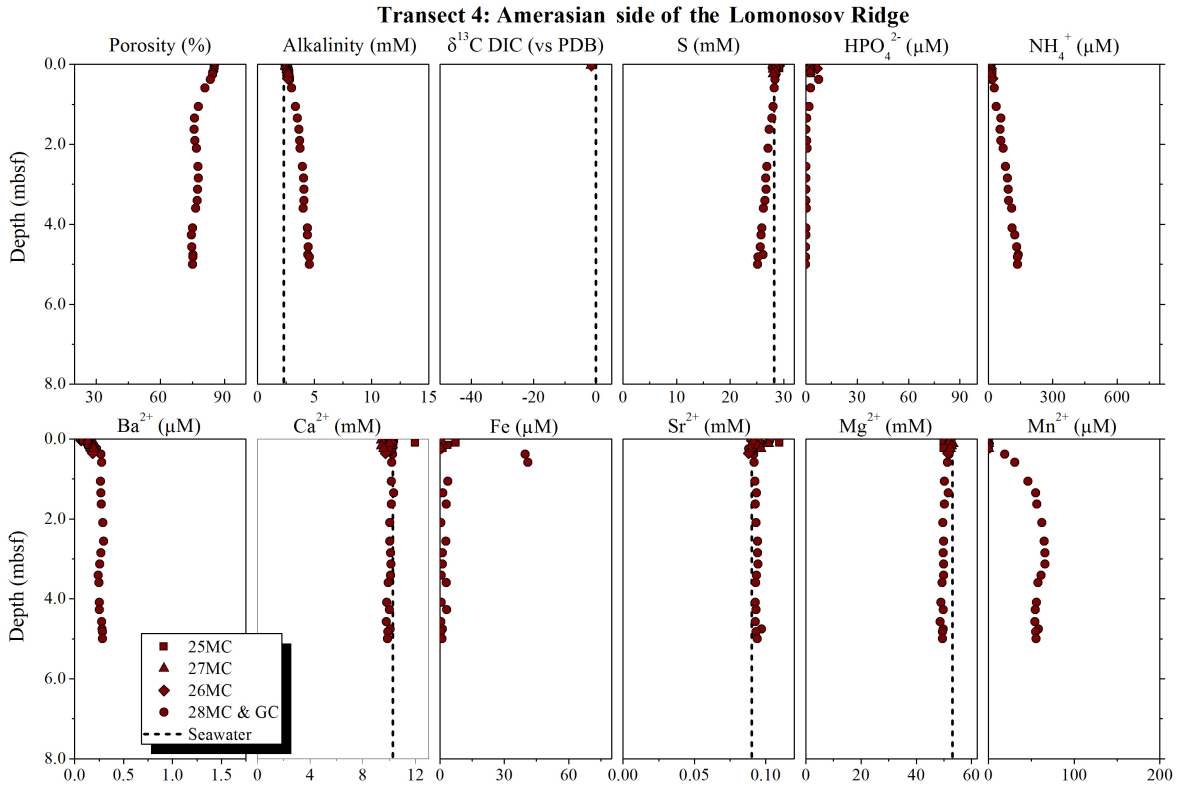

Figure 7. Transect 4 results. IAPSO standard seawater (black dotted line) shown for comparison.

(Eq. 4). Estimated HCO_3^- fluxes ($JHCO_3^-$) do not exceed 6.8 mol m^{-2} kyr^{-1} at any station east of the Lomonosov Ridge (Table 2). For comparison, at sites with abundant CH_4 at depth, $JHCO_3^-$ generally exceeds 30 mol m^{-2} kyr^{-1} above the SMT (Table 2). These extreme fluxes arise because methanogenesis in deeper sediment drives an upward flux of HCO_3^- (Fig. 3) and because AOM contributes additional HCO_3^- and HS^- to pore water at the SMT (Eq. 1).

The δ^{13}C-DIC values of pore water decrease with depth at all stations, almost in concert with the rise in alkalinity, implying no CH_4 production because methanogenesis would increase δ^{13}C-DIC values (Fig. 9c; Whiticar, 1999). Other than Station S31, the lowest value of δ^{13}C-DIC is -25.23 ‰ at 5.5 m at Station S22 (Fig. 6). This is interesting because a series of microbial reactions utilizing POM can lead to higher alkalinity and lower δ^{13}C-DIC values in pore water. The most important of these reactions is organoclastic sulfate reduction (OSR), which can be expressed as (Berner, 1980; Boudreau and Westrich, 1984)

$$2CH_2O + SO_4^{2-} \rightarrow H_2S + 2HCO_3^- . \quad (7)$$

As emphasized previously, methane-charged sediment sequences do occur on continental slopes in the Arctic. Of particular interest to this study are locations in the Beaufort Sea, where indications for gas hydrate manifest on seismic profiles (Grantz et al., 1976, 1982; Weaver and Stewart, 1982; Hart et al., 2011; Phrampus et al., 2014), and pore water profiles have been generated using shallow piston cores (Coffin et al., 2013). Striking contrasts exist between pore water profiles of the Beaufort Sea and those of SNESS (Table 2). In the Beaufort Sea, there are moderate to high downward SO_4^{2-} and upward CH_4 fluxes (1.9 to 154.8 mol m^{-2} kyr^{-1}), shallow SMTs (6.29 to 1.06 mbsf), high DIC fluxes between the SMT and the mud line (46.3 to 242.6), and negative δ13C-DIC values at SMTs (≈ -20 ‰).

5.3 Special case: Lomonosov Ridge station

Station 31 on the Lomonosov Ridge (Fig. 8) differs from all other stations examined in this study. Here, pore water chemistry profiles hint at CH_4 in pore space within shallow sediment. Extrapolation of the dissolved sulfur profile suggests an SMT at approximately 14 mbsf This depth lies within the range common for locations with AOM (D'Hondt et al., 2002), notably including well studied sites on Blake Ridge (Borowski et al., 1999). Similar to some sites with CH_4, the δ^{13}C-DIC values become very "light"; indeed, the value at the base of the core, -43.5 ‰, almost necessitates CH4 oxidation within shallow sediment. Comparably steep alkalinity (1.6 mM m^{-1}) and NH_4^+ gradients (60.4 µM m^{-1}) also characterize most sites with CH_4 near the seafloor. However, there is an issue concerning reduced sulfur, which is a product of AOM (Eq. 1). If AOM was occurring at $\sim$ 13.9 mbsf,

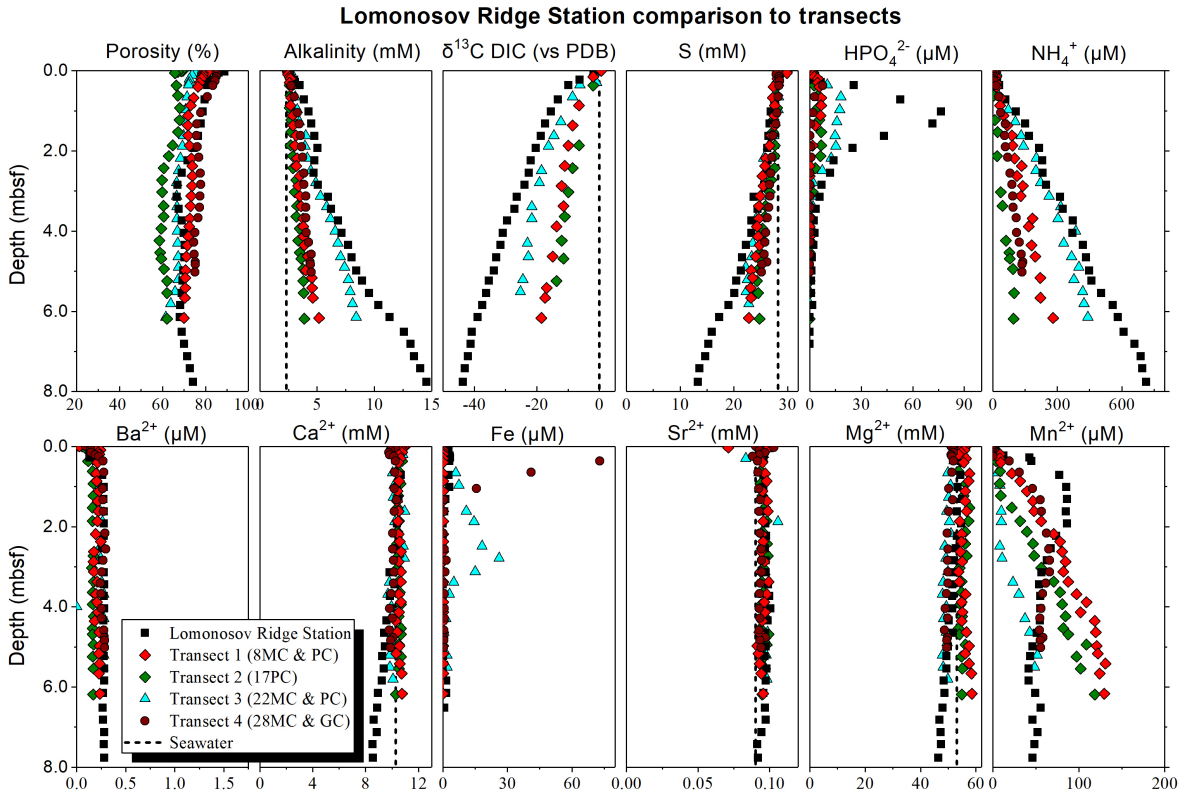

Figure 8. Lomonosov Ridge Station results. IAPSO standard seawater (black dotted line) and representative stations from the four transects shown for comparison.

one might expect evidence for HS^- migrating from below (Fig. 3). No ZnS precipitated in pore waters of this core upon addition of ZnAc.

A comparison of published DIC fluxes, SO_4^{2-} fluxes, and SMT depths (Table 2) reveals that fluxes decrease exponentially with SMT depth (Fig. 11). In fact, a fundamental relationship exists when one considers that upward CH_4 fluxes control the SMT depth (Eq. 1; Fig. 3). The modest SO_4^{2-} flux ($-13.9\,mol\,m^{-2}\,kyr^{-1}$) and alkalinity flux ($11.3\,mol\,m^{-2}\,kyr^{-1}$) estimated for the Lomonosov Ridge station conform to those expected for an SMT at about 14 mbsf For example, Hensen et al. (2003) calculated an SO_4^{2-}- flux of $-14.7\,mol\,m^{-2}\,kyr^{-1}$ for a site with an SMT at 14 mbsf in the Argentine Basin, and Berg (2008) calculated an SO_4^{2-} flux of $-8.05\,mol\,m^{-2}\,kyr^{-1}$ for a site with an SMT at 16 mbsf along the Costa Rica margin.

5.4 Other chemistry

Microbial communities preferentially utilize the most energetically favorable oxidant available, leading to a characteristic reaction sequence in marine sediment (Froelich et al., 1979; Berner, 1980; D'Hondt et al., 2004). With increasing depth below the seafloor, these include aerobic respiration, denitrification, manganese oxide reduction, iron oxide reduction, SO_4^{2-} reduction, and finally methanogenesis. Many of the cores collected across SNESS appear to terminate in the zone of metal oxide reduction. This is because, at most stations, Mn and Fe profiles are still increasing at the bottom of the sampled interval (Figs. 4–8), presumably due to dissimilatory Mn- and Fe-oxide reduction. However, Mn may be more complicated. März et al. (2011) find evidence from Mn profiles along the southern Mendeleev Ridge that suggest diagenetic remobilization of Mn at depth and diffusion toward shallow sediments. The relatively deep depths of metal oxide reduction, nevertheless, are consistent with a relatively low input of POM to the seafloor and completely contrast with most sites where high CH_4 concentrations exist in shallow sediment. A simple interpretation is that there is insufficient input of POC over time to drive methanogenesis near the seafloor.

The station on the Lomonosov Ridge again stands apart. Here, Mn and Fe concentrations reach maxima at 1.3 and 0.5 mbsf, respectively, and decrease below. This is likely due to Mn and Fe produced during dissimilatory oxide reduction, but where both metals precipitate below into carbonate (Mn and Fe) or sulfide phases (Fe; Jørgensen et al., 1990; März et al., 2011). This is common at locations with modest POC input, and the Lomonosov Ridge site appears to receive higher organic carbon burial over time than all the

Table 2. Published and calculated fluxes.

Ocean	Location	Water depth (m)	SMT depth (mbsf)	SO_4^{2-} flux ($mol\,m^{-2}\,kyr^{-1}$)	Alkalinity flux ($mol\,m^{-2}\,kyr^{-1}$)	$\delta^{13}C$ at SMT (‰)
Arctic	Beaufort Sea – Cape Halkett[a,b]	280	1.06	−154.8	242.6	−21.5
Arctic	Beaufort Sea – Cape Halkett[a,b]	342	1.47	−124.7	212.3	−20.2
Arctic	Beaufort Sea – Cape Halkett[a,b]	1005	3.73	−44.2	130.3	−18.2
Arctic	Beaufort Sea – Cape Halkett[a,b]	1458	6.29	−27.4	46.3	−19.7
Arctic	East Siberian slope	349	61	−1.8	1.7	–
Arctic	East Siberian slope	367	25	−6.9	6.3	–
Arctic	East Siberian slope	384	64	−2.4	2.3	–
Arctic	East Siberian slope	524	35	−5.6	2.8	–
Arctic	East Siberian slope	733	58	−2.1	1.5	–
Arctic	East Siberian slope	977	58	−2.1	1.6	–
Arctic	East Siberian slope	964	23	−9.2	6.8	–
Arctic	East Siberian slope	1000	52	−3.3	3.3	–
Arctic	East Siberian slope	1143	44	−5.1	3.5	–
Arctic	East Siberian slope	1120	14	−13.9	11.3	–
Atlantic	New Jersey continental slope[q,i]	912	28.9	−3.3	3.6*	–
Atlantic	Blake Ridge[q,p]	1293	50.3	−3.4	3.8*	–
Atlantic	Blake Ridge[q,p]	1798	26.9	−6.6	4.9*	–
Atlantic	Blake Ridge[q,x]	2567	42.0	−3.8	3.5*	–
Atlantic	Blake Ridge[q,x]	2641	24.5	−7.6	6.9*	–
Atlantic	Blake Ridge[q,x]	2777	21.7	−8.3	5.4*	–
Atlantic	Blake Ridge[q,x]	2770	22.5	−7.8	4.7*	–
Atlantic	Blake Ridge[q,x]	2798	21.5	−8.7	4.4*	–
Atlantic	Blake Ridge[q,p]	2985	9.3	−20.0	20.4*	–
Atlantic	Blake Ridge[q,p]	3481	12.3	−17.1	17.0*	–
Atlantic	Blake Ridge[q,p]	4040	16.8	−10.5	10.8*	–
Atlantic	Gulf of Mexico – Keathley Canyon[w]	1300	9	−33*	17*	-49.6
Atlantic	Gulf of Mexico – Atwater Valley[w]	1300	0.1	−2901	–	–
Atlantic	Gulf of Mexico – Atwater Valley[w]	1300	0.1	−2901	–	–
Atlantic	Gulf of Mexico – Atwater Valley[w]	1300	0.6	−437	–	–
Atlantic	Gulf of Mexico – Atwater Valley[w]	1300	7	−67	–	-46.3
Atlantic	Amazon Fan[q,v,y]	3191	37.2	−3.2	4.1*	−39.8
Atlantic	Amazon Fan[q,v,y]	3474	6.2	−24.6	22.7*	−47.5
Atlantic	Amazon Fan[q,v,y]	3704	3.7	−40.3	24.3*	−49.6
Atlantic	Western Africa[q,z]	426	12.8	−12.5	18.2*	–
Atlantic	Western Africa[q,z]	738	52.9	−3.1	2.9*	–
Atlantic	Western Africa[q,z]	1280	21.3	−12.0	15.6*	−19.8
Atlantic	Western Africa[q,z]	1402	18.3	−14.9	28.3*	–
Atlantic	Western Africa[q,z]	1713	38.5	−5.1	4.1*	–
Atlantic	Western Africa[q,z]	2179	26.7	−7.8	10.4*	–
Atlantic	Western Africa[q,z]	2382	21.1	−18.1	21.8*	–
Atlantic	Western Africa[q,z]	2995	29.7	−14.9	20.9*	–
Atlantic	Argentine Basin[l]	1228	10.5	−19.1	–	–
Atlantic	Argentine Basin[l]	1492	12	−20.2	–	–
Atlantic	Argentine Basin[l]	1568	4.9	−84.6	–	–
Atlantic	Argentine Basin[l]	1789	5.9	−55.6	–	–
Atlantic	Argentine Basin[l]	3247	10	−21.8	–	–
Atlantic	Argentine Basin[l]	3167	14	−14.7	–	–
Atlantic	Argentine Basin[l]	3542	3.7	−75.4	–	–
Atlantic	Argentine Basin[l]	3551	5.6	−39.9	–	–
Atlantic	Argentine Basin[l]	3551	4.1	−93.3	–	–
Atlantic	Argentine Basin[l]	3623	5	−43.1	–	–
Atlantic	Argentine Basin[l]	4280	5.1	−43.5	–	–
Atlantic	Argentine Basin[l]	4799	12	−17.9	–	–
Indian	Oman[q,1]	591	50.2	−2.2	1.1*	–
Indian	Oman[q,1]	804	46.5	−2.8	4.4*	–
Indian	Oman[q,1]	1423	82.4	−1.8	0.8*	–
Pacific	Bering Sea[p,2]	1008	6.3	−32.8	37.8	−25.1
Pacific	Cascadia[q,u,2]	959	9.0	−23.6	–	−23.8
Pacific	Cascadia[q,u,2]	1322	7.9	−21.3	–	−30.8
Pacific	Cascadia[q,u,2]	1828	2.5	−49.0	–	−33.9

Table 2. Continued.

Ocean	Location	Water Depth (m)	SMT Depth (mbsf)	SO_4^{2-} Flux ($mol\,m^{-2}\,kyr^{-1}$)	Alkalinity Flux ($mol\,m^{-2}\,kyr^{-1}$)	$\delta^{13}C$ at SMT (‰)
Pacific	Cascadia – Hydrate Ridge[o]	834	8	−10.9	11.3	−19.6
Pacific	Cascadia – Hydrate Ridge[o]	850	7.65	−22.3	23.2	−30.2
Pacific	Cascadia – Hydrate Ridge[o]	871	7.4	−26.6	33.4	−24.9
Pacific	Cascadia – Hydrate Ridge[g]	896	7.8	−16	22	−22.5
Pacific	Umitaka Spur[h]	900	2.2	−71	114	–
Pacific	Umitaka Spur[h]	947	2.9	−58	80	–
Pacific	Umitaka Spur[h]	1034	2.0	-102	100	–
Pacific	Japan Sea[s,4]	901	10	−33.6	38.4*	–
Pacific	California margin[q,5]	955	13.3	−17.3	19.6*	–
Pacific	California margin[q,5]	1564	19.0	−9.3	12.8*	–
Pacific	California margin[q,5]	1926	31.0	−4.3	3.1*	–
Pacific	Nankai Trough[q,6]	1741	32.2	−4.9	3*	–
Pacific	Nankai Trough[s,6]	2997	11.0	−5.6	8.7*	–
Pacific	Nankai Trough[q,6]	3020	18.2	−7.0	6.4*	–
Pacific	Santa Barbara[k]	587	1.3	−175.2	–	–
Pacific	Soledad[k]	542	1	−310.3	–	–
Pacific	Pescadero[k]	408	1.4	−164.3	–	–
Pacific	Magdalena[k]	600	1.5	−182.5	–	–
Pacific	Alfonso[k]	713	0.8	−474.5	–	–
Pacific	Costa Rica margin[q,7]	3306	16.0	−8.1	9.6*	–
Pacific	Costa Rica margin[q,7]	4177	19.8	−7.5	3.1*	–
Pacific	Costa Rica margin[q,7]	4311	18.6	−12.3	12.4*	–
Pacific	Peru margin[s,8]	161	30	−6.9	–	–
Pacific	Peru margin[t,9]	427	40	−1.2	–	−25.4
Pacific	Peru margin[t,9]	5086	9	−25.0	–	−13.2
Pacific	Chilean Coast[c]	586	5.55	−22.9	–	–
Pacific	Chilean Coast[c]	723	0.33	−362.0	–	–
Pacific	Chilean Coast[c]	980	2.92	−45.3	–	–
Pacific	Chilean Coast[c]	768	10.11	−13.3	–	–
Pacific	New Zealand – Porangahau Ridge[f]	1900–2150	12.8	−11.4	–	−31.4
Pacific	New Zealand – Porangahau Ridge[f]	1900–2150	4.4	−53.3	–	−31.6
Pacific	New Zealand – Porangahau Ridge[f]	1900–2150	3.6	−50.5	–	−31.4
Pacific	New Zealand – Porangahau Ridge[f]	1900–2150	2.1	−74.2	–	−33.4
Pacific	New Zealand – Porangahau Ridge[f]	1900–2150	3.8	−61.5	–	−35.0
Pacific	New Zealand – Porangahau Ridge[f]	1900–2150	1.8	−82.6	–	−48.8
Pacific	New Zealand – Hikurangi[b,d]	350	39.5	5*	7.3*	–
Pacific	New Zealand – Hikurangi[b,d]	332	12.9	19.3*	13.6*	–
Pacific	New Zealand – Hikurangi[b,d]	98	0.87	192.1*	160.9*	–
Pacific	New Zealand – Hikurangi[b,d]	285	3.64	65.2*	59.6*	–
Southern Ocean	Antarctic – Cumberland Bay[n]	237	5.03	−86	95	−25.4
Southern Ocean	Antarctic – Cumberland Bay[n]	260	0.80	-539	291	-23.5
Southern Ocean	Antarctic – Cumberland Bay[n]	275	2.80	−135	116	−15.5

[a] = Coffin et al. (2013); [b] = Richard Coffin (personal communication, 2016); [c] = Coffin et al. (2007); [d] = Coffin et al. (2007b); [e] = Coffin et al. (2008); [f] = Hamdan et al. (2011) and Coffin et al. (2014); [g] = Dickens and Snyder (2009); [h] = Snyder et al. (2007); [i] = Mountain et al. (1994); [j] = Lin et al. (2006); [k] = Berelson et al. (2005); [l] = Hensen et al. (2003); [m] = Dickens (2001); [n] = Geprägs et al. (2016); [o] = Claypool et al. (2006); [p] = Keigwin et al. (1998); [q] = Berg (2008); [r] = Borowski et al. (2000); [s] = D'Hondt et al. (2002); [t] = D'Hondt et al. (2004); [u] = Torres et al. (2009); [v] = Burns (1998); [w] = Kastner et al. (2008a); [x] = Paull et al. (1996); [y] = Flood et al. (1995); [z] = Wefer et al. (1998); [1] = Prell et al. (1998); [2] = Takahashi et al. (2011); [3] = Riedel et al. (2006); [4] = Tamaki et al. (1990); [5] = Lyle et al. (1997); [6] = Moore et al. (2001); [7] = Kimura et al. (1997); [8] = Suess et al. (1988); [9] = D'Hondt et al. (2003). * = calculated from published material.

other locations examined. Given the relationship of alkalinity to ammonia (Fig. 10), much of the organic matter on the continental slope may derive from terrestrial rather than marine sources (Müller and Suess, 1979; Reimers et al., 1992), but a more detailed study of sedimentation rates and organic matter content and composition is required to elucidate these relationships further.

5.5 Signatures of AOM and OSR

Some authors have used changes in DIC and SO_4^{2-} concentrations between the seafloor and the SMT to infer the relative importance of AOM and OSR in marine sediments (Kastner et al., 2008b; Luo et al., 2013; Hu et al., 2015). This idea can be expressed by comparing $\Delta(DIC+Ca^{2+}+Mg^{2+})$ and ΔSO_4^{2-}, where Ca^{2+} and Mg^{2+} are included to account

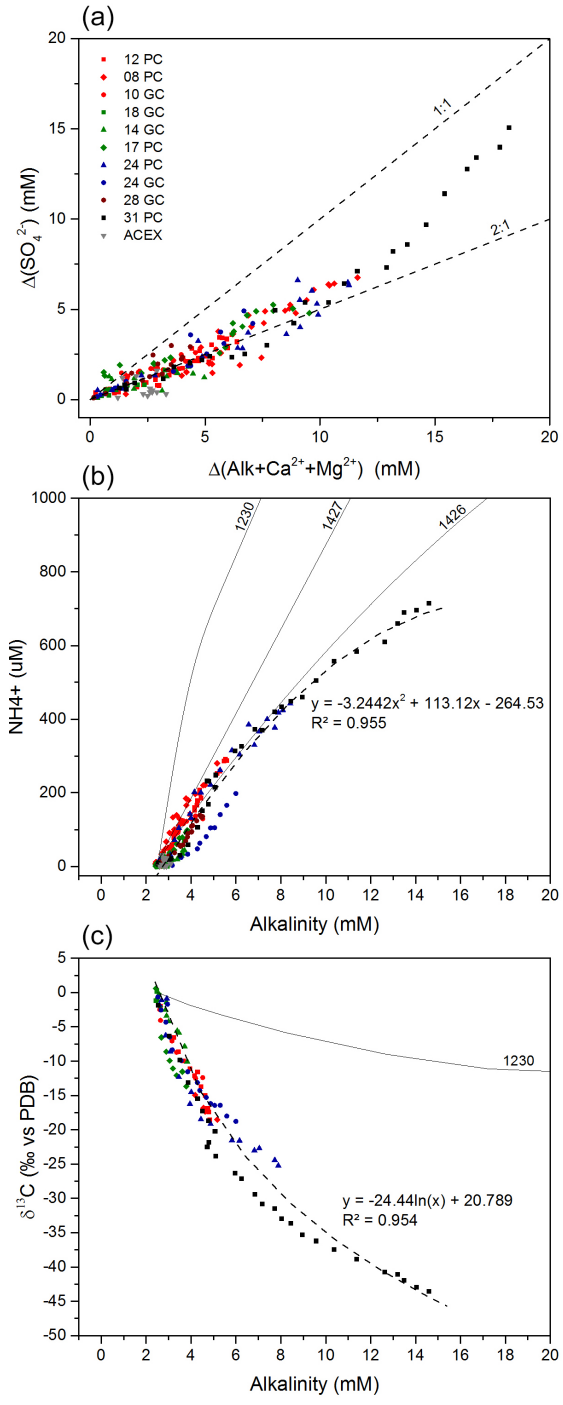

Figure 9. Relationship of **(a)** sulfate change (ΔSO_4^{2-}) and carbonate-corrected alkalinity change ($\Delta Alk + Ca^{2+} + Mg^{2+}$); **(b)** the second order polynomial association of NH_4^+ to Alkalinity; and **(c)** decreasing δ^{13}C-DIC values with alkalinity increase. Methane-charged sites (1230, 1426, and 1427; 1230, Shipboard Scientific Party, 2003; 1426 and 1427, Expedition Scientists, 2014) given for comparison.

for loss of DIC via carbonate precipitation (other authors, such as Snyder et al., 2007, and Wehrmann et al., 2011, use fluxes instead of concentrations). The rationale lies in the fact that the C : S ratio for AOM is 1 : 1 (Eq. 1), whereas the C : S ratio for OSR is 2 : 1 (Eq. 7). However, this approach neglects two considerations: (1) changes in concentration do not directly relate to fluxes, because of differences in diffusivities of various ionic species, and (2) a flux of HCO_3^- from below the SMT can augment the DIC produced from AOM or OSR at or above the SMT (Dickens and Snyder, 2009). Thus, changes in alkalinity relative to SO_4^{2-} often exceed 1 : 1, even at locations completely dominated by AOM (Chatterjee et al., 2011).

Rather than comparing changes in C : S molar ratios or going through detailed flux calculations to interrogate the importance of the two reactions in shallow sediment, one might also incorporate the δ^{13}C-DIC values. This is because δ^{13}C-DIC values and the depth of DIC production differ considerably across many sites where either AOM or OSR dominates. We generate a figure expressing these relationships at multiple sites (Fig. 12), where the y axis is

$$\frac{\Delta\left(\mathrm{DIC} + \mathrm{Ca}^{2+} + \mathrm{Mg}^{2+}\right)}{\Delta\left(\mathrm{SO}_4^{2-}\right)}, \tag{8}$$

and the x axis is DIC $\cdot\, \delta^{13}$C-DIC. The C : S ratios of dissolved species lie above 1 : 1 at most locations, regardless of whether CH_4 exists in shallow sediment and AOM dominates, as highlighted by Chatterjee et al. (2011). However, sites with significant CH_4 have considerably more negative DIC $\cdot\, \delta^{13}$C-DIC values. Notably, pore waters from all stations examined here, except S31 on the Lomonosov Ridge, have modest DIC $\cdot\, \delta^{13}$C-DIC values consistent with a dominance of OSR in shallow sediment rather than AOM.

In summary, from general pore water considerations as well as from comparisons to pore water profiles at other locations, sediments across SNESS do not contain CH_4 over extensive areas of shallow sediment. Implicit in this finding is that sediment sequences in this region lack widespread gas hydrate. As models for gas hydrate occurrence in the Arctic (Fig. 1) correctly predict gas hydrate in several regions (e.g., Kvenvolden and Grantz, 1990; Max and Lowrie, 1993; Max and Johnson, 2012), our findings prompt an interesting question: why are predictions so markedly wrong for the SNESS?

5.6 Possible explanations for widespread absence of gas hydrate and methane

To understand the likely absence of widespread gas hydrates across SNESS, one needs to consider the generalities of their occurrence in marine sediment. There are two basic conditions for gas hydrate on continental slopes (Kvenvolden, 1993; Dickens, 2001). The first consideration is the "potential volume", or the pore space where physiochemical conditions (e.g., temperature, pressure, salinity, sediment poros-

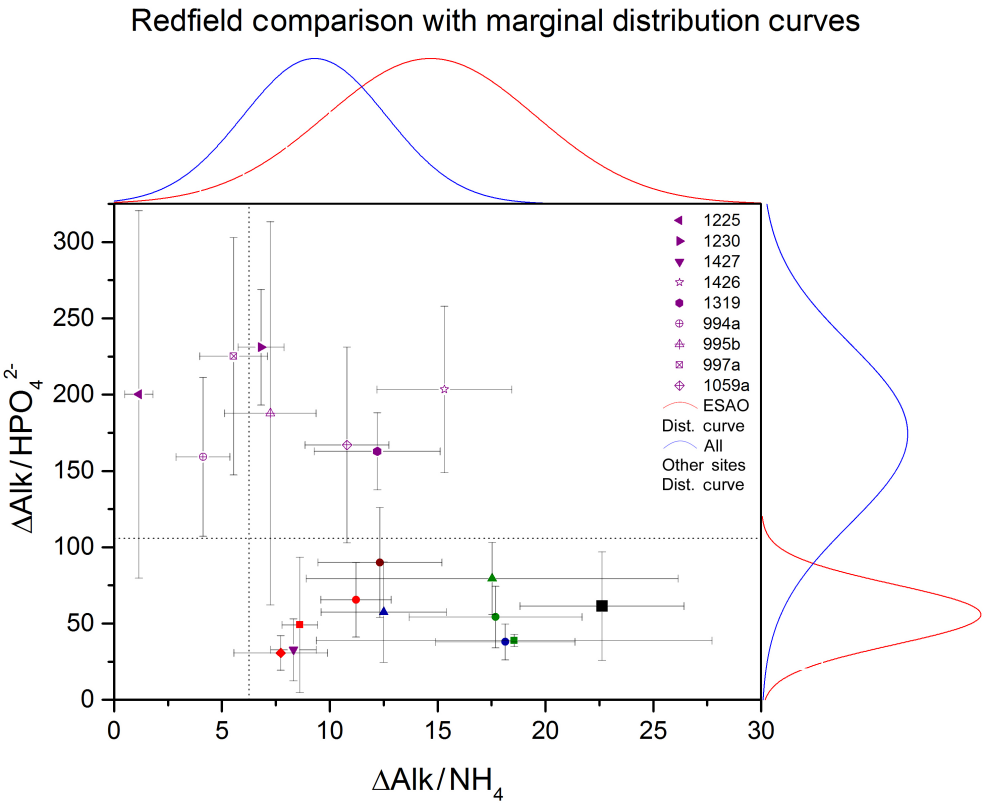

Figure 10. C : N : P ratio indirectly shown with $\Delta Alk / \Delta NH_4^+$ and $\Delta Alk / \Delta HPO_4^{2-}$. Several global sites, 994, 995, 997, 1059, 1225, 1230, 1426, 1427, and 1319 (994–997, 1059, Borowski et al., 2000; 1225 and 1230, Shipboard Scientific Party, 2003; 1426 and 1427, Expedition Scientists, 2014), are given for comparison. Blue marginal distribution curves show global distribution, while red gives SNESS stations (this project). SNESS pore waters have higher C : N and lower C : P than comparative sites.

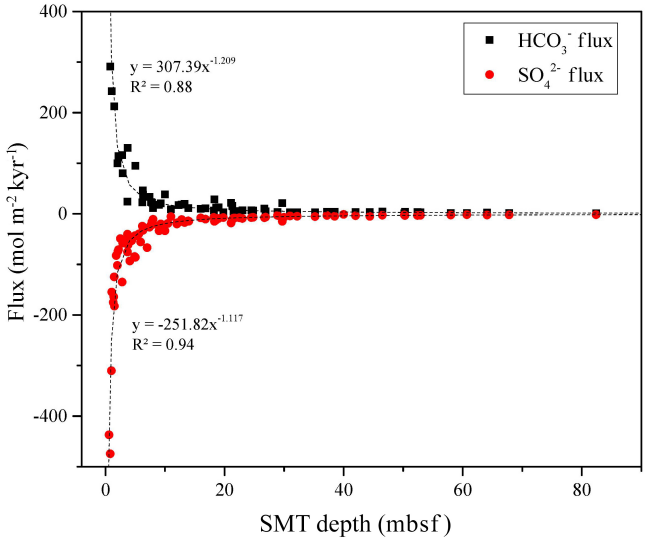

Figure 11. Bicarbonate (HCO_3^-) and sulfate (SO_4^{2-}) flux exponential relationship with SMT depth for all sites listed in Table 2.

ity) are amenable to gas hydrate formation. As stressed in previous works, because of cold bottom water and a low geothermal gradient, the region has a relatively large volume of sediment with appropriate gas hydrate stability conditions (Stranne et al., 2016). The second consideration is the "occupancy", or the fraction of sediment pore space with sufficient CH_4 to precipitate gas hydrate. While environmental conditions across SNESS are highly conducive for gas hydrate formation, pore water profiles strongly indicate little to no CH_4 exists in the upper hundred meters of sediment.

This inference strongly depends on recognition as to how diffusive systems operate in marine sediment. Hundreds of pore water profiles have been generated during scientific ocean drilling expeditions, including scores into CH_4-charged sediment sequences. These profiles almost universally show vertical connectivity of pore water chemistry over hundreds of meters (Fig. 3). Moreover, away from local sites of advection, pore water profiles are generally similar over extensive areas. This occurs because, given sufficient permeability and time, diffusive fluxes transport species from intervals of high concentration to intervals of low concentration. Hence, unless some impermeable layer exists in the sediment sequence, even CH_4 at depth impacts near-seafloor concen-

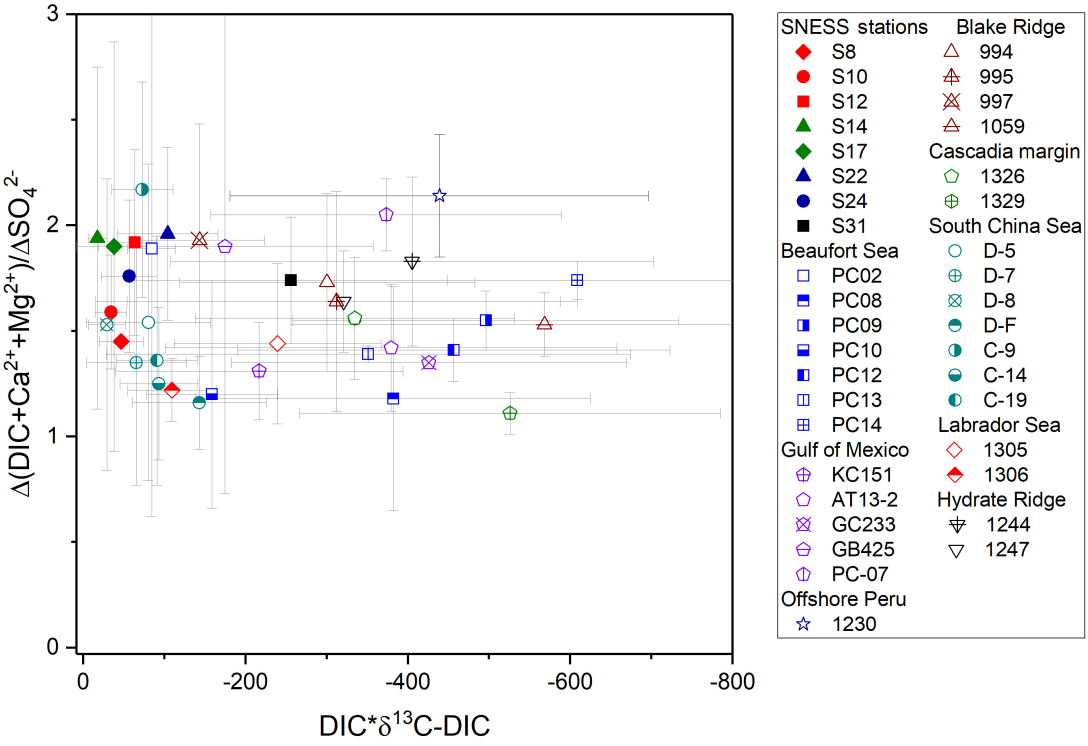

Figure 12. Ratio of carbonate-corrected alkalinity change (ΔAlk+Ca^{2+}+Mg^{2+}) and sulfate change (ΔSO_4^{2-}) to the product of DIC and δ^{13}C-DIC value (AT13-2 and KC151, Kastner et al., 2008a; PC02-PC14, Coffin et al., 2008; 994-997, 1059, Borowski et al., 2000; Paull et al., 2000; 1326 and 1329, Torres and Kastner, 2009; GC233 and GB425, Hu et al., 2010; D-5–D-8 and D-F, Hu et al., 2015; C9–C19, Luo et al., 2013; PC-07, Smith and Coffin, 2014; 1230, Shipboard Scientific Party, 2003; 1244 and 1247, Claypool et al., 2006; 1305 and 1306, Party, 2005, including global sites for comparison) showing the paucity of methane-charged sites actually reaching a 1 : 1 C : S ratio. Error bars are one sigma. SNESS-plotted pore waters substitute alkalinity for DIC. With the absence of sulfide, DIC and alkalinity should be roughly equivalent in these pore waters. SNESS locations use the same symbols as previous figures.

trations. Indeed, work on the outer Blake Ridge wonderfully shows this phenomenon. The uppermost gas hydrate in sediment in this region lies at about 190 mbsf (Borowski et al., 1999). Nonetheless, its presence occurs over $\sim$ 26 000 km^2 and affects shallow pore water profiles across this region, because the flux of CH_4 from depth drives AOM near the seafloor (Borowski et al., 1999; Dickens, 2001).

No seafloor features indicative of seafloor CH_4 expulsion were found during the bathymetric mapping of SNESS. Nonetheless, it is possible that local CH_4 venting, perhaps related to and mediated by bubble transport, could occur away from transects and cores of SWERUS Leg 2. Certainly, the chemistry of advecting fluids toward seafloor features such as mud volcanoes and cold seeps typically differs from the much broader surrounding region (Luff and Wallmann, 2003; Coffin et al., 2007; Hiruta et al., 2009; Hu et al., 2010; Coffin et al., 2014; Hu et al., 2015). However, in such cases, even the encompassing area typically has shallow SMTs. Without invoking odd geology, such as an extensive impermeable layer, it is unlikely that significant CH_4 exists in shallow sediment across much of SNESS, including as gas hydrate or free gas. Here it is stressed that neither gas hydrate nor free gas can exist in sediment on continental slopes without high concentrations of dissolved gas in surrounding pore water (Dickens et al., 1997; Hiruta et al., 2009; Geprägs et al., 2016). The surprising lack of CH_4 across SNESS, as inferred from pore water profiles, suggests insufficient net input of POC over time, so that either methanogenesis has not occurred or the product has been lost.

The accumulation of POC within the SNESS region may be relatively low over the Plio–Pleistocene. With low POC inputs, other microbial reactions can exhaust the labile organic matter needed for methanogenesis. This may, in fact, explain why the pore water chemistry suggests that metal oxide reduction dominates the geochemical environment at most of our stations. Without further investigation, we offer four possibilities (not mutually exclusive) as to why this might occur: (1) significant sea-ice concentrations, both at present-day and during past glacial intervals, greatly diminishes primary production of marine organic carbon within the water column; (2) the extremely broad continental shelf prevents large accumulations of terrestrial organic-rich sediment from reaching the slope; (3) highly variable sediment accumulation, perhaps corresponding to glacial–interglacial os-

cillations, creates a situation where POC from either source is consumed during time intervals of low deposition; and, although not directly related to POC accumulation, (4) changes in sea level during the last glacial maximum caused much of the hydrate to outgas as the stability zone moved downslope (Stranne et al., 2016). With the third explanation, large land-based glaciers in the past may have physically scoured sediment (and organic matter) from the upper slope (Jakobsson et al., 2014). Importantly, the first three explanations distinguish the SNESS region from the Beaufort Sea, where abundant CH_4 in shallow sediment unquestionably occurs (Coffin et al., 2011; Treude et al., 2014).

In earlier times, particularly the Cretaceous through early Eocene (Jenkyns et al., 2004; Sluijs et al., 2006; Backman et al., 2009), organic-rich sediment may have accumulated at high rates throughout the Arctic. In the Lomonosov Ridge in the central Arctic, lower Eocene sediments definitely contain high organic carbon and potential indicators of past methanogenesis (e.g., barium mobilization). As these cores contain no CH_4 at present day, if CH_4 was generated, it has presumably been lost in the intervening time. Should these organic-rich horizons be buried across the SNESS region and presently generating CH_4 via thermogenesis, the gas is too deeply buried to affect shallow sediment.

6 Conclusions

Leg 2 of the SWERUS-C3 expedition recovered sediments and pore waters from numerous stations across the continental slopes north of the East Siberian Sea. These stations extend from Wrangel Island to the New Siberian Islands and provide information from a climatically sensitive but highly inaccessible area.

In an effort to understand CH_4 cycling within the SNESS region, we generated detailed pore water profiles of multiple dissolved constituents. The pore water profiles are coherent and interpretable and give a general view: most stations have low SO_4^{2-} and HCO_3^- fluxes (< 6.2 and $6.8\,\mathrm{mol\,m^{-2}\,kyr^{-1}}$, respectively), a moderate decrease in δ^{13}C-DIC values with depth ($-3.6\,‰\,\mathrm{m^{-1}}$ average), no dissolved H_2S, a moderate rise in HPO_4^{2-} and NH_4^+ concentrations, and slightly decreasing Ca^{2+}, Mg^{2+}, and Sr^{2+} concentrations. Except for one station on the Lomonosov Ridge, metal oxide reduction appears to be the dominant geochemical environment affecting shallow sediment, and there is no evidence for upward diffusing CH_4. These results strongly suggest that gas hydrates do not occur on any of our depth transects spread across the continental slope in this region of the Arctic Ocean. This directly conflicts with ideas in multiple publications, which generally have assumed large quantities of CH_4 and gas hydrate. However, it remains possible that significant CH_4 occurs where the Lomonosov Ridge intersects the continental margin as well as westward on the Laptev Sea continental slope.

Data availability. All data is available within this paper (Tables 1 and 2) and in the Supplement (Tables S1, S2, and S3).

The Supplement related to this article is available online at https://doi.org/10.5194/bg-14-2929-2017-supplement.

Competing interests. The authors declare that they have no conflict of interest.

Acknowledgements. The authors would like to thank the SWERUS-C3 Leg 2 crew as well as reviewers.

Edited by: Örjan Gustafsson
Reviewed by: two anonymous referees

References

Aagaard, K. and Carmack, E. C.: The role of sea ice and other fresh water in the Arctic Circulation, J. Geophys. Res., 94, 14485–14498, 1989.

Aagaard, K., Coachman, L. K., and Carmack, E. C.: On the halocline of the Arctic Ocean, Deep Sea Res., 28, 529–545, 1981.

Aharon, P. and Fu, B.: Microbial sulfate reduction rates and sulfur and oxygen isotope fractionations at oil and gas seeps in deepwater Gulf of Mexico, Geochim. Cosmochim. Ac., 64, 233–246, 2000.

Alperin, M. J., Reeburgh, W. S., and Whiticar, M. J.: Carbon and hydrogen isotope fractionation resulting from anaerobic methane oxidation, Global Biogeochem. Cy., 2, 279–288, 1988.

Archer, D.: A model of the methane cycle, permafrost, and hydrology of the Siberian continental margin, Biogeosciences, 12, 2953–2974, https://doi.org/10.5194/bg-12-2953-2015, 2015.

Augstein, E.: Die Expedition ARCTIC'96 mit FS Polarstern(ARK XII) mit der Arctic Climate System Study (ACSYS); The expedition ARCTIC'96 of RV Polarstern (ARK XII) with the Arctic Climate System Study (ACSYS). Berichte zur Polarforschung (Reports on Polar Research), 234, 1997.

Backman, J. and Moran, K.: Expanding the Cenozoic paleoceanographic record in the Central Arctic Ocean: IODP Expedition 302 Synthesis: Central European J. Geosci., 1, 157–175, 2009.

Bakhmutov, V., Whitledge, T., Wood, K., and Ostrovskiy, A.: Report on the execution of marine research in the Bering Strait, East Siberian and the Chukchi Sea by the Russian-American Expedition under the program of "RUSALCA" during the period from 23 August through 30 September, 2009.

Barnes, R. O. and Goldberg, E. D.: Methane production and consumption in anoxic marine sediments, Geol., 4, 297–300, 1976.

Beaudoin, Y. C., Waite, W., Boswell, R., and Dallimore, S. R.: Frozen Heat: A UNEP Global Outlook on Methane Gas Hydrates, Volume 1, UN, Environ. Programme, GRID-Arendal, 2014.

Berelson, W. M., Prokopenko, M., Sansone, F. J., Graham, A. W., McManus, J., and Bernhard, J. M.: Anaerobic diagenesis of silica and carbon in continental margin sediments: discrete zones of

TCO 2 production, Geochim. Cosmochim. Ac., 69, 4611–4629, 2005.

Berg, P., Risgaard-Petersen, N., and Rysgaard, S.: Interpretation of measured concentration profiles in sediment pore water, Limnol. Oceanogr., 43, 1500–1510, 1998.

Berg, R. D.: Diffusional methane fluxes within continental margin sediments and depositional constraints on formation factor estimates, ProQuest, 2008.

Berner, R. A.: Diagenetic models of dissolved species in the interstitial waters of compacting sediments, Am. J. Sci., 275, 88–96, 1975.

Berner, R. A.: Stoichiometric models for nutrient regeneration m anoxic sediment?, Limnology, 22, 781–786, 1977.

Berner, R. A.: Early Diagenesis: A Theoretical Approach, Princeton University Press, Princeton, N.J., 1980.

Bhatnagar, G., Chatterjee, S., Chapman, W. G., Dugan, B., Dickens, G. R., and Hirasaki G. J.: Analytical theory relating the depth of the sulfate-methane transition to gas hydrate distribution and saturation, Geochem. Geophy. Geosy., 12, 1–21, 2011.

Biastoch, A., Treude, T., Ruepke, L. H., Riebesell, U., Roth, C., Burwicz, E. B., Park, W., Latif, M., Boening, C. W., Madec, G., and Wallmann, K.: Rising Arctic Ocean temperatures cause gas hydrate destabilization and ocean acidification, Geophys. Res. Lett., 38, 1–5, 2011.

Boetius, A., Ravenschlag, K., Schubert, C. J., Rickert, D., Widdel, F., Gieseke, A., Amann, R., Jørgensen, B. B., Witte, U., and Pfannkuche, O.: A marine microbial consortium apparently mediating anaerobic oxidation of methane, Nature, 407, 623–626, 2000.

Borowski, W. S., Paull, C. K., and Ussler III, W.: Marine porewater sulfate profiles indicate in situ methane flux from underlying gas hydrate, Geol., 24, 655–658, 1996.

Borowski, W. S., Paull, C. K., and Ussler W. III: Global and local variations of interstitial sulfate gradients in deepwater, continental margin sediments: Sensitivity to underlying methane and gas hydrates, Mar. Geol., 159, 131–154, 1999.

Borowski, W. S., Hoehler, T. M., Alperin, M. J., Rodriguez, N. M., and Paull, C. K.: Significance of anaerobic methane oxidation in methane-rich sediments overlying the Blake Ridge gas hydrates, in: Proceedings of the ocean drilling program, scientific results, 164, 87–99, 2000.

Borowski, W. S., Cagatay, N., Ternois, Y., and Paull, C. K.: Data Report: carbon isotopic composition of dissolved CO_2, CO_2 gas, and methane, Blake –Bahama Ridge and Northeast Bermuda Rise, ODP Leg 172, in: Proceedings of the ODP. Scientific Results (College Station, TX), edited by: Keigwin, L. D., Rio, D., Acton, G. D., and Arnold, E., 172, 1–16, 2001.

Boudreau, B. P.: Diagenetic models and their implementation (Vol. 505), Berlin, Springer, 1997.

Boudreau, B. P. and Westrich, J. T.: The dependence of bacterial sulfate reduction on sulfate concentration in marine sediments, Geochim. Cosmochim. Ac., 48, 2503–2516, 1984.

Buffett, B. and Archer, D.: Global inventory of methane clathrate: sensitivity to changes in the deep ocean, Earth Planet. Sc. Lett., 227, 185–199, 2004.

Burns, S. J.: Carbon isotopic evidence for coupled sulfate reduction-methane oxidation in Amazon Fan sediments, Geochim. Cosmochim. Ac., 62, 797–804, 1998.

Carcione, J. M. and Tinivella, U.: Bottom-simulation reflectors: Seismic velocities and AVO effects, Geophysics, 65, 54–67, 2000.

Chatterjee, S., Dickens, G. R., Bhatnagar, G., Chapman, W. G., Dugan, B., Snyder, G. T., and Hirasaki, G. J.: Pore water sulfate, alkalinity, and carbon isotope profiles in shallow sediment above marine gas hydrate systems: A numerical modeling perspective, J. Geophys. Res-Sol. Ea., 116, 1–25, 2011.

Claypool, G. E. and Kvenvolden, K. A.: Methane and other hydrocarbon gases in marine sediment, Annu. Rev. Earth Pl. Sc., 11, 299–327, 1983.

Claypool, G. E., Milkov, A. V., Lee, Y. J., Torres, M. E., Borowski, W. S., and Tomaru, H.: Microbial Methane Generation and Gas Transport in Shallow Sediments of an Accretionary Complex, Southern Hydrate Ridge (ODP Leg 204), Offshore Oregon USA, in: Proceedings of the ODP, Scientific Results, edited by: Trehu, A. M., Bohrmann, G., Torres, M. E., and Colwell, F. S., Ocean Drilling Program, College Station, Texas, 2006.

Cline, J. D.: Spectrophotometric determination of hydrogen sulfide in natural waters, Limnol. Oceanogr., 14, 454–458, 1969.

Coffin, R. B., Pohlman, J. W., Gardner, J., Downer, R., Wood, W., Hamdan, L., Walker, S., Plummer, R., Gettrust, J., and Diaz, J.: Methane hydrate exploration on the mid Chilean coast: a geochemical and geophysical survey, J. Petrol. Sci. Eng., 56, 32–41, 2007a.

Coffin, R., Hamdan, L., Pohlman, J., Wood, W., Pecher, I., Henrys, S., Greinert, J., and Faure, K.: Geochemical characterization of concentrated gas hydrate deposits on the Hikurangi Margin, New Zealand, Preliminary Geochemical Cruise Report, NRL/MR/ 6110-07, 2007b.

Coffin, R. B., Hamdan, L. J., Plummer, R., Smith, J., Gardner, J., Hagen, R., and Wood, W.: Analysis of Methane and Sulfate Flux in Methane-charged Sediments from the Mississippi Canyon, Gulf of Mexico, Mar. Petrol. Geol., 25, 977–987, 2008.

Coffin, R. B., Plummer, R. B., Yoza, B., Larsen, R. K., Millholland, L. C., and Montgomery, M. T.: Spatial variation in shallow sediment methane sources and cycling on the Alaskan Beaufort Sea Shelf/Slope, Mar. Petrol. Geol., 45, 186–197, 2013.

Coffin, R. B., Hamdan, L. J., Smith, J. P., Rose, P. S., Plummer, R. E., Yoza, B., Pecher, I., and Montgomery, M. T.: Contribution of vertical methane flux to shallow sediment carbon pools across Porangahau ridge, New Zealand, Energies, 7, 5332–5356, 2014.

Collett, T. S., Lee, M. W., Agena, W. F., Miller, J. J., Lewis, K. A., Zyrianova, M. V., Boswell, R., and Inks, T. L.: Permafrost associated natural gas hydrate occurrences on the Alaska North Slope, Mar. Petrol. Geol., 28, 279–294, 2010.

Danyushevskaya, A., Yashin, D. S., and Kirillow, O. V.: Geochemical patterns of distribution of organic carbon in the bottom sediments of Arctic seas, Oceanology, 20, 183–188, 1980.

Darby, D. A., Naidu, A. S., Mowatt, T. C., and Jones, G.: Sediment composition and sedimentary processes in the Arctic Ocean, in: The Arctic Seas: Climatology, Oceanography, Geology and Biology, edited by: Herman, Y., Van Nostrand Reinhold, New York, 657–720, 1989.

Dickens, G. R.: Sulfate profiles and barium fronts in sediment on the Blake Ridge. Present and past methane fluxes through a large gas hydrate reservoir, Geochim. Cosmochim. Ac., 65, 529–543, 2001.

Dickens, G. R. and Snyder, G. T.: Interpreting upward methane flux from marine pore water profiles, In: Fire in the Ice, NETL Methane Hydrate Newsletter, 9, 7–10, 2009.

Dickens, G. R., Paull, C. K., and Wallace, P.: Direct measurement of in situ methane quantities in a large gas hydrate reservoir, Nature, 385, 426–428, 1997.

Dickens, G. R., Koelling, M., Smith, D. C., Schnieders, L., and the IODP Expedition 302 Scientists: Rhizon Sampling of Pore Waters on Scientific Drilling Expeditions: An Example from the IODP Expedition 302, Arctic Coring Expedition (ACEX), Sci. Dril., 4, 22–25, https://doi.org/10.2204/iodp.sd.4.08.2007, 2007.

D'Hondt, S., Rutherford, S., and Spivack, A. J.: Metabolic activity of subsurface life in deep-sea sediments, Science, 295, 2067–2070, 2002.

D'Hondt, S., Jørgensen, B. B., Miller, D. J., Batzke, A., Blake, R., Cragg, B. A., Cypionka, H., Dickens, G. R., Ferdelman, T., Hinrichs, K. U. and Holm, N. G.: Distributions of microbial activities in deep subseafloor sediments, Science, 306, 2216–2221, 2004.

D'Hondt, S. L., Jørgensen, B. B., Miller, D. J., and Shipboard Scientific Pary: Proceedings of the Ocean Drilling Program, Initial Reports Volume 201, 2003.

Dmitrenko, I. A., Polyakov, I. V., Kirillov, S. A., Timokhov, L. A., Frolov, I. E., Sokolov, V. T., Simmons, H. L., Ivanov, V. V., and Walsh, D.: Toward a warmer Arctic Ocean: spreading of the early 21st century Atlantic Water warm anomaly along the Eurasian Basin margins, J. Geophys. Res.-Oceans, 113, 1–13, 2008.

Dmitrenko, I. A., Bauch, D., Kirillov, S. A., Koldunov, N., Minnett, P. J., Ivanov, V. V., Hölemann, J. A., and Timokhov, L. A.: Barents Sea upstream events impact the properties of Atlantic water inflow into the Arctic Ocean: Evidence from 2005 to 2006 downstream observations, Deep-Sea Res. Pt.I, 56, 513–527, 2009.

Donohue, C. M., Snyder, G. T., and Dickens, G. R.: Data report: major cation concentrations of interstitial waters collected from deep sediments of Eastern Equatorial Pacific and Peru Margin (ODP Leg 201), Proceedings of ODP, Scientific Results, 201, Ocean Drilling Program, College Station, TX, 2006.

Dymond, J., Suess, E., and Lyle, M.: Barium in deep-sea sediment: A geochemical proxy for paleoproductivity, Paleoceanography, 7, 163–181, 1992.

Elliott, S., Maltrud, M., Reagan, M., Moridis, G., and Cameron-Smith P.: Marine methane cycle simulations for the period of early global warming, J. Geophys. Res-Biogeo., 116, 1–13, 2011.

Engen, Ø., Faleide, J. I., and Dyreng, T. K.: Opening of the Fram Strait gateway: A review of plate tectonic constraints, Tectonophysics, 450, 1–69, 2008.

Expedition 346 Scientists: Asian Monsoon: onset and evolution of millennial-scale variability of Asian monsoon and its possible relation with Himalaya and Tibetan Plateau uplift, IODP Preliminary Report, 346, 2014.

Ferré, B., Mienert, J., and Feseker, T.: Ocean temperature variability for the past 60 years on the Norwegian-Svalbard margin influences gas hydrate stability on human time scales, J. Geophys. Res., 117, 1–14, 2012.

Flood, R. D., Piper, D. J. W., Klaus, A., and Scientific Research Party: Proceedings of the Ocean Drilling Program, Initial Reports, 155: College Station, TX (Ocean Drilling Program), 1995.

Froelich, P., Klinkhammer, G. P., Bender, M. A. A., Luedtke, N. A., Heath, G. R., Cullen, D., Dauphin, P., Hammond, D., Hartman, B., and Maynard, V.: Early oxidation of organic matter in pelagic sediments of the eastern equatorial Atlantic: suboxic diagenesis, Geochim. Cosmochim. Ac., 43, 1075–1090, 1979.

Geprägs, P., Torres, M. E., Mau, S., Kasten, S., Römer, M., and Bohrmann, G.: Carbon cycling fed by methane seepage at the shallow Cumberland Bay, South Georgia, sub-Antarctic, Geochem. Geophy. Geosy., 17, 1401–1418, 2016.

Gieskes, J. M. and Rogers, W. C.: Alkalinity determination in interstitial waters of marine sediments, J. Sediment. Res., 43, 272–277, 1973.

Gieskes, J. M., Gamo, T., and Brumsack, H.: Chemical methods for interstitial water analysis aboard JOIDES Resolution, 1991.

Gingele, F. and Dahmke, A.: Discrete barite particles and barium as tracers of paleoproductivity in South Atlantic sediments, Paleoceanography, 9, 151–168, 1994.

Giustiniani, M., Tinivella, U., Jakobosson, M., and Rebesco, M.: Arctic Ocean gas hydrate stability in a changing climate, J. Geol. Res., 116, 1–10, https://doi.org/10.1155/2013/783969, 2013.

Goldhaber, M.: Kinetic Models of Sulfur Diagenesis in Recent Marine Sediments, In Transactions-AGU, 55, 696–697, 1974.

Grantz, A., Boucher, G., and Whitney, O. T.: Possible solid gas hydrate and natural gas deposits beneath the continental slope of the Beaufort Sea, U.S. Geological Survey Circulation Number 733, 1976.

Grantz, A., Mann, D. M., and May, S. D.: Tracklines of multichannel seismic-reflection data collected by the U.S. Geological Survey in the Beaufort and Chukchi Seas in 1977 for which profiles and stack tapes are available, U.S. Geological Survey Open-File Report 1982, 82–735, 1982.

Greinert, J., Bohrmann, G., and Suess, E.: Gas hydrate-associated carbonates and methane-venting at Hydrate Ridge: classification, distribution, and origin of authigenic lithologies, Natural gas hydrates: Occurrence, distribution, and detection, 99–113, 2001.

Haacke, R. R., Westbrook, G. K., and Riley, M.: Controls on the formation and stability of gas hydrate-related bottom-simulating reflectors (BSRs): a case study from the west Svalbard continental slope, J. Geophys. Res., 113, 1–17, 2008.

Hamdan, L. J., Gillevet, P. M., Pohlman, J. W., Sikaroodi, M., Greinert, J., and Coffin, R. B.: Diversity and biogeochemical structuring of bacterial communities across the Porangahau ridge accretionary prism, New Zealand, FEMS Microbiol. Ecol., 77, 518–532, 2011.

Haraldsson, C., Anderson, L. G., Hassellöv, M., Hulth, S., and Olsson, K.: Rapid, high-precision potentiometric titration of alkalinity in ocean and sediment pore waters, Deep Sea Res. Pt. I, 44, 2031–2044, 1997.

Hart, P. E., Pohlman, J. W., Lorenson, T. D., and Edwards, B. D.: Beaufort Sea Deep-water gas hydrate recovery from a seafloor mound in a region of widespread BSR occurrence, in: Proceedings of the 7th International Conference on Gas Hydrates (ICGH 2011), Edinburgh, Scotland, 2011.

Hensen, C., Zabel, M., Pfiefer, K., Schwenk, T., Kasten, S., Riedinger, N., Schulz, H. D., and Boetius, A.: Control of sulfate porewater profiles by sedimentary events and the significance of anaerobic oxidation of methane for the burial of sulfur in marine sediments, Geochim. Cosmochim. Ac., 67, 2631–2647, 2003.

Hiruta, A., Snyder, G. T., Tomaru, H., and Matsumoto, R.: Geochemical constraints for the formation and dissociation of gas hydrate in an area of high methane flux, eastern margin of the Japan Sea, Earth Planet. Sc. Lett., 279, 326–339, 2009.

Holbrook, W. S., Hoskins, H., Wood, W. T., Stephen, R. A., and Lizarralde, D.: Methane hydrate and free gas on the Blake ridge from vertical seismic profiling, Science, 273, 1840–1843, 1996.

Holler, T., Wegener, G., Knittel, K., Boetius, A., Brunner, B., Kuypers, M. M., and Widdel, F.: Substantial 13C/12C and D/H fractionation during anaerobic oxidation of methane by marine consortia enriched in vitro, Environ. Microbiol. Rep., 1, 370–376, 2009.

Holmes, R. M., McClelland, J. W., Peterson, B. J., Shiklomanov, I. A., Shiklomanov, A. I., Zhulidov, A. V., Gordeev, V. V., and Bobrovitskaya, N. N.: A circumpolar perspective on fluvial sediment flux to the Arctic Ocean, Global Biogeochem. Cy., 16, 1–14, 2002.

Hu, X., Cai, W.-J., Wang, Y., Luo, S., and Guo, X.: Pore-water geochemistry of two contrasting brine-charged seep stations in the northern Gulf of Mexico continental slope, Mar. Geochem., 118, 99–107, 2010.

Hu, Y., Feng, D., Liang, Q., Xia, Z., Chen, L., and Chen, D.: Impact of anaerobic oxidation of methane on the geochemical cycle of redox-sensitive elements at cold-seep stations of the northern South China Sea, Deep Sea Res. Pt. II, 122, 84–94, https://doi.org/10.1016/j.dsr2.2015.06.012, 2015.

Hustoft, S., Bünz, S., Mienert, J., and Chand, S.: Gas hydrate reservoir and active methane-venting province in sediments on <20 Ma young oceanic crust in the Fram Strait, offshore NW-Svalbard, Earth Planet. Sc. Lett., 284, 12–24, 2009.

Hyndman, R. D. and Dallimore, S. R.: Natural gas hydrates studies, Canada Recorder, 26, 11–20, 2001.

Iversen, N. and Jørgensen, B. B.: Diffusion coefficients of sulfate and methane in marine sediments: Influence of porosity, Geochim. Cosmochim. Ac., 57, .571–578, 1993.

Jakobsson, M.: Hypsometry and volume of the Arctic Ocean and its constituent seas: Geochem. Geophy. Geosy., 3, 1–18, 2002.

Jakobsson, M., Backman, J., Rudels, B., Nycander, J., Frank, M., Mayer, L., Jokat, W., Sangiorgi, F., O'Regan, M., Brinkhuis, H., King, J., and Moran, K.: The early Miocene Onset of a Ventilated Circulation Regime in the Arctic Ocean, Nature, 447, 986–990, 2007.

Jakobsson, M., Mayer, L., Coakley, B., Dowdeswell, J. A., Forbes, S., Fridman, B., Hodnesdal, H., Noormets, R., Pedersen, R., Rebesco, M., Schenke, H. W., Zarayskaya, Y., Accettella, D., Armstrong, A., Anderson, R. M., Bienhoff, P., Camerlenghi, A., Church, I., Edwards, M., Gardner, J. V., Hall, J. K., Hell, B., Hestvik, O., Kristoffersen, Y., Marcussen, C., Mohammad, R., Mosher, D., Nghiem, S. V., Pedrosa, M. T., Travaglini, P. G., and Weatherall, P.: The International Bathymetric Chart of the Arctic Ocean (IBCAO) Version 3.0: Geophys. Res. Lett., 39, L12609, https://doi.org/10.1029/2012GL052219, 2012.

Jakobsson, M., Andreassen, K., Bjarnadóttir, L. R., Dove, D., Dowdeswell, J. A., England, J. H., Funder, S., Hogan, K., Ingólfsson, Ó., Jennings, A., Krog-Larsen, N., Kirchner, N., Landvik, J. Y., Mayer, L., Möller, P., Niessen, F., Nilsson, J., O'Regan, M., Polyak, L., Nørgaard-Pedersen, N., and Stein, R.: Arctic Ocean glacial history, Quaternary Sci. Rev., 92, 40–67, 2014.

Jenkyns, H. C., Forster, A., Schouten, S., and Sinninghe Damsté, J. S.: High temperatures in the Late Cretaceous Arctic Ocean, Nature, 432, 888–892, 2004.

Jokat, W.: The expedition of the Research Vessel "Polarstern" to the Arctic in 2009 (ARK-XXIV/3), Berichte zur Polar-und Meeresforschung (Reports on Polar and Marine Research), 615, 2010.

Jokat, W. and Ickrath, M.: Structure of ridges and basins off East Siberia along 81° N, Arctic Ocean, Mar. Petrol. Geol., 64, 222–232, 2015.

Jørgensen, B. B., Bang, M., and Blackburn, T. H.: Anaerobic mineralization in marine sediments from the Baltic Sea-North Sea transition, Mar. Ecol.-Prog. Ser., 59, 39–54, 1990.

Jørgensen, B. B., Weber, A., and Zopfi, J.: Sulfate reduction and anaerobic methane oxidation in Black Sea sediments, Deep Sea Res. Pt I, 48, 2097–2120, 2001.

Jørgensen, B. B., Böttcher, M. E., Lüschen, H., Neretin, L. N., and Volkov, I. I.: Anaerobic methane oxidation and the deep H2S sink generate isotopically heavy sulfides in Black Sea sediments, Geochim. Cosmochim. Ac., 68, 2095–2118, 2004.

Joye, S. B., Boetius, A., Orcutt, B. N., Montoya, J. P., Schulz, H. N., Erickson, M. J., and Lugo, S. K.: The anaerobic oxidation of methane and sulfate reduction in sediments from Gulf of Mexico cold seeps, Chem. Geol., 205, 219–238, 2004.

Kastner, M., Claypool, G., and Robertson, G.: Geochemical constraints on the origin of the pore fluids and gas hydrate distribution at Atwater Valley and Keathley Canyon, northern Gulf of Mexico, Mar. Petr. Geol., 25, 860–872, 2008a.

Kastner, M., Torres, M., Solomon, E., and Spivack, A. J.: Marine pore fluid profiles of dissolved sulfate; do they reflect in situ methane fluxes?, in: Fire in the Ice, NETL Methane Hydrate Newsletter, Summer, 2008b.

Keigwin, L. D., Rio, D., Acton, G. D., and Shipboard Scientific Party: Proceedings of the Ocean Drilling Program, Initial Reports, 172: College Station, TX (Ocean Drilling Program), 1998.

Kimura, G., Silver, E. A., Blum, P., and Shipboard Scientific Party: Proceedings of the Ocean Drilling Program, Initial Reports, vol. 170, 1997.

Klauda, J. B. and Sandler, S. I.: Global distribution of methane hydrate in ocean sediment, Energy Fuel, 19, 469–78, 2005.

Klump, J. V. and Martens, C. S.: Biogeochemical cycling in an organic rich coastal marine basin—II. Nutrient sediment-water exchange processes, Geochim. Cosmochim. Ac., 45, 101–121, 1981.

Kvenvolden, K. A.: Gas hydrates: Geological perspective and global change, Rev. Geophys., 31, 173–187, 1993.

Kvenvolden, K. A. and Grantz, A.: Gas hydrates in the Arctic Ocean region, in The Arctic Ocean Region, Geology of North America, Geol. Soc. of Am., Boulder, Colo., 539–549, 1990.

Kvenvolden, K. A. and Lorenson, T. D.: The global occurrence of natural gas hydrate, in: Natural Gas Hydrates: Occurrence, Distribution, and Detection, edited by: Paull, C. K. and Dillon, W. P., AGU Geophy. Monograph Ser., 124, 3–18, 2001.

Laberg, J. S. and Andreassen, K.: Gas hydrate and free gas indications within the Cenozoic succession of the Bojornya Basin, western Barents Sea, Mar. Petrol. Geol., 13, 921–940, 1996.

Laberg, J. S., Andreassen, K., and Knutsen, S. M.: Inferred gas hydrate on the Barents Sea shelf a model for its formation and a volume estimate, Geo-Mar. Lett., 18, 26–33, 1998.

Lerman, A.: Migrational processes and chemical reactions in Sulfate profiles and barium fronts in sediment 539 interstitial waters, in: The Sea, Volume VI, editd by: Goldberg, E. D., Wiley, New York, 695–738, 1977.

Li, Y.-H. and Gregory, S.: Diffusion of ions in sea sediments, Geochim. Cosmochim. Ac., 38, 703–714, 1974.

Lin, S., Hsieh, W. C., Lim, Y. C., Yang, T. F., Liu, C. S., and Wang, Y.: Methane migration and its influence on sulfate reduction in the Good Weather Ridge region, South China Sea continental margin sediments, Terr. Atmos. Ocean. Sci., 17, 883–902, 2006.

Lorenson, T. D. and Kvenvolden, K. A.: Methane in coastal seawater, sea ice, and bottom sediments, Beaufort Sea, Alaska, USGS Open-File Report 95–70, 1995.

Løvø, V., Elverhøi, A., Antonsen, P., Solheim, A., and Liestøl, O.: Submarine permafrost and gas hydrates in the northern Barents Sea, Norsk Polarinstitutt Rapportserie, 56, 171 pp., 1990.

Luff, R. and Wallmann, K.: Fluid flow, methane fluxes, carbonate precipitation and biogeochemical turnover in gas hydrate-bearing sediments at hydrate ridge, Cascadia margin: numerical modeling and mass balances, Geochim. Cosmochim. Ac., 67, 3403–3421, 2003.

Luo, M., Chen, L., Wang, S., Yan, W., Wang, H., and Chen, D.: Pockmark activity inferred from pore water geochemistry in shallow sediments of the pockmark field in southwestern Xisha Uplift, northwestern South China Sea, Mar. Petrol. Geol., 2013, 247–259, 2013.

Lyle, M., Koizumi, I., Richter, C., and Shipboard Scientific Party: Proceedings of the Ocean Drilling Program, Initial Reports, Vol. 167, 1997.

Majorowicz, J. A. and Osadetz, K. G.: Gas hydrate distribution and volume in Canada, AAPG Bulletin, 85, 1211–1230, 2001.

Makogon, Y. F.: Natural gas hydrates – A promising source of energy, J. Nat. Gas Sc. Eng., 2, 49–59, 2010.

März, C., Stratmann, A., Matthiessen, J., Meinhardt, A. K., Eckert, S., Schnetger, B., Vogt, C., Stein, R., and Brumsack, H. J.: Manganese-rich brown layers in Arctic Ocean sediments: composition, formation mechanisms, and diagenetic overprint, Geochim. Cosmochim. Ac., 75, 7668–7687, 2011.

Max, M. D. and Johnson, A. H.: Natural Gas Hydrate (NGH) Arctic Ocean potential prospects and resource base, OTC Arctic Technology Conference, 27–53, 2012.

Max, M. D. and Lowrie, A.: Natural gas hydrates: Arctic and Nordic Sea potential. Arctic geology and petroleum potential, proceedings of the Norwegian Petroleum Society conference, 15–17 August 1990, Tromsø, Norway. No. 2. Elsevier Science Ltd., 1993.

McGuire, A. D., Anderson, L. G., Christensen, T. R., Dallimore, S., Guo, L. D., Hayes, D. J., Heimann, M., Lorenson, D. D., MacDonald, R. W., and Roulet, N.: Sensitivity of the carbon cycle in the Arctic to climate change, Ecol. Monogr., 79, 523–555, 2009.

Miles, P. R.: Potential distribution of methane hydrate beneath the European continental margins, Geophys. Res. Lett., 22, 3179–3182, 1995.

Miller, M. D., Adkins, J. F., and Hodell, D. A.: Rhizon sampler alteration of deep ocean sediment interstitial water samples, as indicated by chloride concentration and oxygen and hydrogen isotopes, Geochem. Geophy. Geosy., 15, 2401–2413, 2014.

Moore, G. F., Taira, A., and Klaus, A., and Shipboard Scientific Party: Proceedings of the Ocean Drilling Program, Initial Reports Volume 190, 2001.

Moran, K., Backman, J., Brinkhuis, H., Clemens, S. C., Cronin, T., Dickens, G. R., Eynaud, F., Gattacceca, J., Jakobsson, M., Jordan, R. W., and Kaminski, M.: The Cenozoic palaeoenvironment of the arctic ocean, Nature, 441, 601–605, 2006.

Mountain, G. S., Miller, K. G., Blum, P., and Shipboard Scientific Party: Proc. ODP, Initial Reports, 150: College Station, TX (Ocean Drilling Program), 1994.

Müller, P. J. and Suess, E.: Productivity, sedimentation rate, and sedimentary organic matter in the oceans – I. Organic carbon preservation, Deep Sea Res. Pt. A, 26, 1347–1362, 1979.

Murray, R. W., Miller, D. J., and Kryc, K. A.: Analysis of major and trace elements in rocks, sediments, and interstitial waters by inductively coupled plasma–atomic emission spectrometry (ICP-AES), ODP Technical Note 29, 2000.

Niewohner, C., Hensen, C., Kasten, S., Zabel, M., and Schulz, H. D.: Deep sulfate reduction completely mediated by anaerobic methane oxidation in sediments of the upwelling area off Namibia, Geochim. Cosmochim. Ac., 62, 455–464, 1998.

Nöthen, K. and Kasten, S.: Reconstructing changes in seep activity by means of pore water and solid phase Sr/Ca and Mg/Ca ratios in pockmark sediments of the Northern Congo Fan, Mar. Geol., 287, 1–13, 2011.

O'Regan, M., Williams, C. J., Frey, K. E., and Jakobsson, M.: A synthesis of the long-term paleoclimatic evolution of the Arctic, Oceanography, 24, 66–80, 2011.

O'Regan, M., Preto, P., Stranne, C., Jakobsson, M., and Koshurnikov, A.: Surface heat flow measurements from the East Siberian continental slope and southern Lomonosov Ridge, Arctic Ocean, Geochem. Geophy. Geosy., 17, 1–15, 2016.

Ostanin, I., Anka, Z., di Primio, R., and Bernal, A.: Hydrocarbon plumbing systems above the Snøhvit gas field: structural control and implications for thermogenic methane leakage in the Hammerfest Basin, SW Barents Sea, Mar. Petrol. Geol., 43, 127–146, 2013.

Paull, C. K., Ussler III, W., and Dillon, W. P.: Is the extent of glaciation limited by marine gas-hydrates?, Geophys. Res. Lett., 18, 432–434, 1991.

Paull, C. K., Matsumoto, R., Wallace, P. J., and Shipboard Scientific Party: Proceedings of the IODP, Initial Reports, Volume 164: College Station, TX, USA, 1996.

Paull, C. K, Lorenson, T. D., Borowski, W. S., Ussler III, W., Olsen, K., and Rodriguez, N. M.: Isotopic composition of CH_4, CO_2 species, and sedimentary organic matter within samples from the Blake Ridge: gas source implications, in: Proceedings of the ODP, edited by: Paull, C. K., Matsumoto, R., Wallace, P. J., and Dillon, W. P., Sci. Res., 164, 67–78, 2000.

Pecher, I. A., Kukowski, N., Huebscher, C., Greinert, J., and Bialas, J.: The link between bottom-simulating reflections and methane flux into the gas hydrate stability zone – new evidence from Lima Basin, Peru Margin, Earth Planet. Sc. Lett., 185, 343–354, 2001.

Peterson, B. J., Holmes, R. M., McClelland, J. W., Vorosmarty, C. J., Lammers, R. B., Shiklomanov, A. I., Shiklomanov, I. A., and Rahmstorf, S.: Increasing river discharge to the Arctic Ocean, Science, 298, 2171–2173, 2002.

Phrampus, B. J., Hornbach, M. J., Ruppel, C. D., and Hart P. E.: Widespread gas hydrate instability on the upper US Beaufort margin, J. Geophys. Res-Sol. Ea., 119, 8594–8609, 2014.

Piñero, E., Marquardt, M., Hensen, C., Haeckel, M., and Wallmann, K.: Estimation of the global inventory of methane hydrates in marine sediments using transfer functions, Biogeosciences, 10, 959–975, https://doi.org/10.5194/bg-10-959-2013, 2013.

Pohlman, J. W., Riedel, M., Waite, W., Rose, K., and Lapham, L.: Application of Rhizon samplers to obtain high-resolution

pore-fluid records during geo-chemical investigations of gas hydrate systems, Fire in the Ice: Methane Hydrate Newsletter, US Department of Energy/National Energy Technology Laboratory, Fall, 2008.

Polyakov, I. V., Pnyushkov, A. V., and Timokhov, L. A.: Warming of the Intermediate Atlantic Water of the Arctic Ocean in the 2000s, J. Climate, 25, 8362–8370, 2012.

Posewang, J. and Mienert, J.: High-resolution seismic studies of gas hydrates west of Svalbard, Geo-Mar. Lett., 19, 150–156, 1999.

Prell, W. L., Niitsuma, N., and Shipboard Scientific Party: Proceedings of the Ocean Drilling Program, Initial Reports, 117: College Station, TX (Ocean Drilling Program), 1998.

Rachor, E.: The expedition ARK-XI/1 of RV "Polarstern" in 1995: [ARK XI/1, Bremerhaven-Tromsø-, 07.07. 1995-20.09. 1995]. Berichte zur Polarforschung (Reports on Polar Research), 226, 1995.

Reagan, M. T. and Moridis, G. J.: Dynamic response of oceanic hydrate deposits to ocean temperature change, J. Geophys. Res., 113, 1–21, 2008.

Reagan, M. T. and Moridis, G. J.: Large-scale simulation of methane hydrate dissociation along the West Spitsbergen margin, Geophys. Res. Lett., 36, 1–5, 2009.

Redfield, A. C.: The biological control of chemical factors in the environment, Am. Sci., 46, 221–230, 1958.

Reeburgh, W. S.: Methane consumption in Cariaco Trench waters and sediments, Earth Planet Sci. Lett., 28, 337–344, 1976.

Reimers, C. E., Jahnke, R. A. and McCorkle, D. C.: Carbon fluxes and burial rates over the continental slope and rise off central California with implications for the global carbon cycle, Global Biogeochem. Cy., 6, 199–224, 1992.

Riedel, M., Collett, T. S., Malone, M. J., and the Expedition 311 Scientists Proceedings of the Integrated Ocean Drilling Program, Volume 311, 2006.

Riedinger, N., Kasten, S., Gröger, J., Franke, C., and Pfeifer, K.: Active and buried authigenic barite fronts in sediments from the Eastern Cape Basin, Earth Planet. Sc. Lett., 241, 876–887, 2006.

Riedinger, N., Formolo, M. J., Lyons, T. W., Henkel, S., Beck, A., and Kasten, S.: An inorganic geochemical argument for coupled anaerobic oxidation of methane and iron reduction in marine sediments, Geobiology, 12, 172–181, 2014.

Rudels, B., Muench, R. D., Gunn, J., Schauer, U., and Friedrich, H. J.: Evolution of the Arctic Ocean boundary current north of the Siberian shelves, J. Marine Syst., 25, 77–99, 2000.

Ryan, W. B. F., Carbotte, S. M., Coplan, J. O., O'Hara, S., Melkonian, A., Arko, R., Weissel, R. A., Ferrini, V., Goodwillie, A., Nitsche, F., Bonczkowski, J., and Zemsky, R.: Global Multi-Resolution Topography synthesis, Geochem. Geophys. Geosyst., 10, 1–9, 2009.

Schrum, H. N., Murray, R. W., and Gribsholt, B.: Comparison of Rhizon Sampling and Whole Round Squeezing for Marine Sediment Porewater, Sci. Dril., 13, 47–50, https://doi.org/10.2204/iodp.sd.13.08.2011, 2012.

Schulz, H. D.: Quantification of early diagenesis: dissolved constituents in marine pore water, Springer Berlin Heidelberg, Mar. Geochem., 85–128, 2000.

Seeberg-Elverfeldt, J., Schlüter, M., Feseker, T., and Kölling, M.: Rhizon sampling of pore waters near the sediment/water interface of aquatic systems, Limnol. Oceanogr.-Meth., 3, 361–371, 2005.

Seifert, R. and Michaelis, W.: Organic compounds in sediments and pore waters of Sites 723 and 724, in: Proc. ODP, Sci. Results, 117: College Station, TX (ODP), 529–545, 1991.

Semiletov, I., Makshtas, O. A., Akasofu, S. I., and Andreas, E. L.: Atmospheric CO_2 balance: the role of Arctic sea ice, Geophys. Res. Lett., 31, 1–4, 2004.

Serreze, M. C., Walsh, J. E., Chapin III, F. S., Osterkamp, T., Dyurgerov, M., Romanovsky, V., Oechel, W. C., Morison, J., Zhang T., and Barry, R. B.: Observational evidence of recent change in the northern high-latitude environment, Climatic Change, 46, 159–207, 2000.

Shakhova, N., Semiletov, I., Salyuk, A., Yusupov, V., Kosmach, D., and Gustafsson, Ö.: Extensive Methane venting to the atmosphere from sediments of the East Siberian arctic shelf, Science, 327, 1246–1250, 2010a.

Shakhova, N., Semiletov, I., Leifer, I., Rekant, P., Salyuk, A., and Kosmach, D.: Geochemical and geophysical evidence of methane release from the inner East Siberian Shelf, J. Geophys. Res., 115, 1–14, 2010b.

Shipboard Scientific Party: Leg 201 summary, in: Proc. ODP, Init. Repts., 201: College Station TX (Ocean Drilling Program), 1–81, 2003.

Sluijs, A., Schouten, S., Pagani, M., Woltering, M., Brinkhuis, H., Damsté, J. S. S., Dickens, G. R., Huber, M., Reichart, G. J., Stein, R. and Matthiessen, J.: Subtropical Arctic Ocean temperatures during the Palaeocene/Eocene thermal maximum, Nature, 441, 610–613, 2006.

Smith, J. P. and Coffin, R. B.: Methane Flux and Authigenic Carbonate in Shallow Sediments Overlying Methane Hydrate Bearing Strata in Alaminos Canyon, Gulf of Mexico, Energies, 7, 6118–6141, 2014.

Snyder, G. T., Hiruta, A., Matsumoto, R., Dickens, G. R., Tomaru, H., Takeuchi, R., Komatsubara, J., Ishida, Y., and Yu, H.: Porewater profiles and authigenic mineralization in shallow marine sediments above the methane-charged system on Umitaka Spur, Japan Sea, Deep-Sea Res. Pt. II, 54, 1216–1239, 2007.

Soloviev, V. A.: Gas-hydrate-prone areas of the ocean and gas-hydrate accumulations, Journal of the Conference Abstracts, 6, p. 158, 2002.

Spencer, A. M., Embry, A. F., Gautier, D. L., Stoupakova, A. V., and Sørensen, K.: An overview of the petroleum geology of the Arctic. Geological Society, London, Memoirs, 35, 1–15, 2011.

Spielhagen, R. F., Werner, K., Sorensen, S. A., Zamelczyk, K., Kandiano, E., Budeus, G., Husum, K., Marchitto, T. M., and Hald, M.: Enhanced modern heat transfer to the Arctic by warm Atlantic water, Science, 331, 450–453, 2011.

Stein, R.: Arctic Ocean sediments: processes, proxies, and paleoenvironment, Developments in Mar. Geol., 2. Elsevier, Amsterdam, 592, 2008.

Stein, R., Boucsein, B., and Meyer, H.: Anoxia and high primary production in the Paleogene central Arctic Ocean: First detailed records from Lomonosov Ridge, Geophys. Res. Lett., 33, 1–6, 2006.

Stranne, C., O'Regan, M., Dickens, G. R., Crill, P., Miller, C., Preto, P., and Jakobsson, M.: Dynamic simulations of potential methane release from East Siberian continental slope sediments, Geochem. Geophy. Geosy., 17, 872–886, 2016.

Stroeve, J. C., Serreze, M. C., Holland, M. M., Kay, J. E., Malanik, J., and Barrett, A. P.: The Arctic's rapidly shrinking sea ice cover: a research synthesis, Climatic Change, 110, 1005–1027, 2012.

Suess, E., von Huene, R., and Shipboard Scientific Party: Proceedings of the Ocean Drilling Program, Initial Reports, 112: College Station, TX (Ocean Drilling Program), 1988.

Takahashi, K., Ravelo, A. C., Alvarez Zarikian, C. A., and the Expedition 323 Scientists Proceedings of the Integrated Ocean Drilling Program, Volume 323, 2011.

Takahashi, T. Broecker, V. S., and Langer, S.: Redfield ratio based on chemical data from isopycnal surfaces, J. Geophys. Res.-Oceans, 90, 6907–6924, 1985.

Tamaki, K., Pisciotto, K., Allan, J., and Shipboard Scientific Party: Proceedings of the Ocean Drilling Program, Initial Reports, Vol. 127, 1990.

Thatcher, K. E., Westbrook, G. K., Sarkar, S., and Minshull, T. A.: Methane release from warming?induced hydrate dissociation in the West Svalbard continental margin: Timing, rates, and geological controls, J. Geophys. Res.-Sol. Ea., 118, 22–38, 2013.

Tian, H., Chen, G., Zhang, C., Melillo, J. M., and Hall, C. A.: Pattern and variation of C:N:P ratios in China's soils: a synthesis of observational data, Biogeochem., 98, 139–151, 2010.

Torres, M. E. and Kastner M.: Data report: Clues about carbon cycling in methane-bearing sediments using stable isotopes of the dissolved inorganic carbon, IODP Expedition 311, Proceedings of the IODP, 311, 2009.

Torres, M. E., McManus, J., Hammond, D. E., De Angelis, M. A., Heeschen, K. U., Colbert, S. L., Tryon, M. D., Brown, K. M., and Suess, E.: Fluid and chemical fluxes in and out of sediments hosting methane hydrate deposits on Hydrate Ridge, OR, I: Hydrological provinces, Earth Planet. Sc. Lett., 201, 525–540, 2002.

Torres, M. E., Kastner, M., Wortmann, U. G., Colwell, F., and Kim, J.: Estimates of methane production rates based on δ13C of the residual DIC in pore fluids from the Cascadia margin, EOS, 8(52), Fall Meet. Suppl., Abstract GC14A04, 2007.

Treude, T., Krause, S., Maltby, J., Dale, A. W., Coffin, R., and Hamdan, L. J.: Sulfate reduction and methane oxidation activity below the sulfate-methane transition zone in Alaskan Beaufort Sea continental margin sediments: Implications for deep sulfur cycling, Geochim. Cosmochim. Ac., 144, 217–237, 2014.

Ussler, W. and Paull, C. K.: Rates of anaerobic oxidation of methane and authigenic carbonate mineralization in methane-rich deep-sea sediments inferred from models and geochemical profiles, Earth Planet. Sc. Lett., 266, 271–287, 2008.

Wallmann, K., Pinero, E., Burwicz, E., Haeckel, M., Hensen, C., Dale, A. W., and Ruepke, L.: The global inventory of methane hydrate in marine sediments: A theoretical approach, Energies, 5, 2449–2498, 2012.

Weaver, J. S. and Stewart, J. M.: In-situ hydrates under the Beaufort Sea Shelf, in: Proceedings of the Fourth Canadian Permafrost Conference 1981, edited by: French, M. H., Roger J. E. Brown Memorial Volume, Nat. Res. Council Can., Ottawa, Ont., 312–319, 1982.

Wefer, G., Berger, W. H., Richter, C., and Shipboard Scientific Party: Proceedings of the Ocean Drilling Program, Initial Reports, 175, College Station, TX (Ocean Drilling Program), 1998.

Wehrmann, L. M., Risgaard-Petersen, N., Schrum, H. N., Walsh, E. A., Huh, Y., Ikehara, M., Pierre, C., D'Hondt, S., Ferdelman, T. G., Ravelo, A. C., and Takahashi, K.: Coupled organic and inorganic carbon cycling in the deep subseafloor sediment of the northeastern Bering Sea Slope (IODP Exp. 323), Chem. Geol., 284, 251–261, 2011.

Whiticar, M. J.: Carbon and hydrogen isotope systematics of bacterial formation and oxidation of methane, Chem. Geol., 161, 291–314, 1999.

Xu, D., Wu, W., Ding, S., Sun, Q. and Zhang, C.: A high-resolution dialysis technique for rapid determination of dissolved reactive phosphate and ferrous iron in pore water of sediments, Sci. Total Environ., 421, 245–252, 2012.

Yamamoto, K. and Dallimore, S.: Aurora-JOGMEC-NRCan Mallik 2006–2008 Gas Hydrate Research Project progress, in: Fire in the Ice, NETL Methane Hydrate Newsletter, Summer 2008, 1–5, 2008.

Ye, H., Yang, T., Zhu, G., Jiang, S., and Wu, L.: Pore water geochemistry in shallow sediments from the northeastern continental slope of the South China Sea, Mar. Petrol. Geol., 75, 68–82, 2016.

Yoshinaga, M. Y., Holler, T., Goldhammer, T., Wegener, G., Pohlman, J. W., Brunner, B., Kuypers, M. M., Hinrichs, K. U., and Elvert, M.: Carbon isotope equilibration during sulphate-limited anaerobic oxidation of methane, Nat. Geosci., 7, 190–194, 2014.